Fuel 347 (2023) 128310

Contents lists available at ScienceDirect

Fuel

journal homepage: www.elsevier.com/locate/fuel

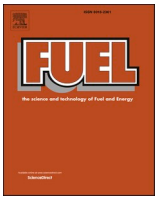

Kinetics of combustion of lignocellulosic biomass: recent research and critical issues

Osvalda Senneca [a,*], Francesca Cerciello [b]

[a] Istituto di Scienze e Tecnologia per l'Energia e la Mobilità Sostenibili (STEMS)-CNR, 80125 Napoli, Italy
[b] Laboratory of Industrial Chemistry, Ruhr University Bochum, 44801 Bochum, Germany

ARTICLE INFO

Keywords:
Lignocellulosic biomass
Kinetic analysis
TGA
Combustion
Oxy-combustion

ABSTRACT

Predicting biomass combustion at temperatures of practical interest requires kinetic expression robust and reliable over a large temperature range.

The present work examines experimental works on combustion kinetics of lignocellulosic biomass published since 2015 and reports the experimental methods used and the kinetic parameters obtained therein. The most common experimental strategy, used in 39 referenced works, was non-isothermal thermogravimetric analysis, yet the kinetic parameters obtained varied by order of magnitude.

The large variability of the kinetic parameters found in literature cannot be only explained by the feedstock heterogeneity or the different data analysis methods. One possible and apparently neglected source of error lies in the fact lignocellulosic biomasses are complex materials, constituted by different components, thus thermogravimetric curves are the resultant of multiple and partly overlapping stages of mass loss. Kinetic analysis in this case easily generates errors. Another criticality that the work wants to emphasize is the fact that biomass pyrolyses, burns and even thermally anneals throughout a TGA experiment. These progressive structural changes are a further problem for application of conventional kinetic analysis methods.

Altogether, it can be concluded that it is difficult to obtain from conventional TGA analysis reliable kinetic expressions of biomass combustion to be used for boilers modelling. For complex materials like biomass, it is recommended to adopt expert-case sensitive approaches. As an example, the case of walnut shells combustion is presented. For this material, four components with different combustion reactivity have been identified and simplified single rate kinetics are proposed according to the temperature interval of interest.

1. Introduction

In the current energy scenario, dominated by the concern for global climate change, lignocellulosic biomass are natural candidates to replace coal in traditional combustion applications, in particular in power plants for heat and electricity, in cement and steel making etc.

If the biomass is produced with a short life cycle, it can be considered a carbon neutral energy source; moreover, if Bio-Energy is coupled with CO_2 Capture and Storage (BECCS), even negative CO_2 emissions can be achieved. Notably the Intergovernmental Panel on Climate Change in its report of 2018 has pointed out that negative CO_2 emissions will be most likely indispensable to limit global warming to 1.5 °C and BECCS, among the other options, appears to be most promising in terms of maturity, potential, costs and risks [1]. This perspective sets new challenges for combustion scientists, committed to secure a smooth transition from coal to biomass in a wide range of combustion applications and from conventional to capture ready combustion conditions, such as oxy-combustion.

A huge literature has been produced over the last decades on thermochemical conversion of biomass. A selection of recent and less recent, but still highly cited, reviews on different aspects and issues related is reported in Table 1 [2–26].

The scope of the present work is to highlight the difficulties in derivation and selection of appropriate combustion kinetic expressions, especially if these have to be implemented in predictive tools of models of biomass burners, which operate at high temperature.

In fact, over the last decade, thermogravimetric analysis affirmed itself as the elective and most common technique for the assessment of biomass combustion kinetics, however the validity of such kinetic expressions under realistic operating conditions has not been sufficiently

* Corresponding author.
E-mail address: osvalda.senneca@stems.cnr.it (O. Senneca).

https://doi.org/10.1016/j.fuel.2023.128310
Received 29 September 2022; Received in revised form 6 March 2023; Accepted 2 April 2023
Available online 26 April 2023

Table 1
Review papers on different topics of interest for biomass conversion.

Authors, publication year	Topic	Ref.
Abanades et al. (2021)	Solar reactors applied to biomass	[2]
Álvarez et al. [3]	Oxy-fuel carbon capture technology for pulverized fuel boilers	[3]
Anca-Couce [4]	Reaction mechanisms and modelling of pyrolysis	[4]
Babu [5]	Biofuels, bioproducts and biorefining	[5]
Cai et al. (2018)	Modeling of ash formation and deposition in PF[1] fired boilers	[6]
Choi et al. [7]	Kinetic modeling and CFD[2]	[7]
Dernbecher et al. [8]	Application of CFD[2] in modeling biomass combustion systems	[8]
Di Blasi [10]	Modeling chemical and physical processes of pyrolysis	[9]
Di Blasi [9]	Combustion and gasification rates	[10]
Fatehi et al. [11]	Modeling and optical studies of single particle combustion	[11]
Haberle et al. [12]	Numerical models for biomass particles for domestic appliances	[12]
Hosseini et al. (2019)	Fixed bed combustion modeling	[13]
Kleinhans et al. [14]	Ash formation and deposition	[14]
Leng et al. [15]	Nitrogen transformation	[15]
Lewandowski et al. [16]	Thermal biomass conversion	[16]
Mazaheri et al. [17]	Numerical simulation of biomass gasification	[17]
Miao et al. [18]	Modeling biomass gasification in circulating fluidized beds.	[18]
Niu et al. (2015)	Ash-related issues during biomass combustion	[19]
Pourkashanian et al. [20]	Modeling of coal and biomass combustion in power plants	[20]
Rabaçal et al. [21]	Pulverized combustion of non-woody residues	[21]
Sharifzadeh et al. [22]	Fast pyrolysis and bio-oil upgrading	[22]
Van de Velden et al. [23]	CFB[3] combustion of coal, biomass and sludge	[23]
Verma et al. (2018)	Upgrading of lignin-derived products	[24]
Wang et al. [25]	Chemical kinetic mechanisms of lignocellulosic biomass pyrolysis	[25]
Wang et al. (2021)	Thermochemical processing of biomass and solid wastes	[26]

[1] Pulverized fuel; [2]Computational fluid dynamic; [3]Circulating fluidized bed.

discussed.

The present work surveys 39 recent papers on biomass combustion kinetics and summarizes the methods used in each paper, both in the experimental campaign and for the kinetic analysis. The kinetic expressions suggested in such 39 papers are then compared in order to highlight the large discrepancies between the results.

Ultimately, the limits of a conventional approach for derivation of appropriate and reliable biomass combustion kinetics are discussed and a different method is proposed and applied to a specific biomass.

2. Combustion kinetics by TGA in published papers

This section summarizes the results and the experimental methods used in 39 papers published since 2015, where TGA has been applied to derive biomass combustion kinetics. The selection of kinetic studies [27–65] has been reported in Table 2. Notably a large array of biomass samples has been screened, so forth further contributing to the already large database of biomass combustion kinetics.

2.1. Methods

From the experimental point of view, a TGA campaign can consist of isothermal experiments (I-TGA) at different temperature and non-isothermal experiments (NI-TGA), where the temperature is increased at different constant heating rates. Mass loss data and their derivatives as a function of time/temperature provide the so called TG and derivative DTG curves. The thermogravimetric experiments can be preceded by a pre-treatment stage even in different apparati.

In general two experimental approaches can be followed, schematized as *pathA* and *pathB* +*C* in Fig. 1.

According to *pathA*, thermogravimetric experiments are carried out on the raw biomass in oxidizing atmosphere. In this case, the experimental matrix of the TGA campaign consists of several experiments at different heating rate, typically in the range 2–50 K/min.

According to *pathB* + *C*, the biomass is previously subject to thermal treatment (*B*), which can be torrefaction (*B*.1), pyrolysis (*B*.2) or even torrefaction followed by pyrolysis (*B*.3). Notably the torrefaction and pyrolysis stages can be carried out in the TGA apparatus itself, or else in external reactors such as fixed beds (FR), fluidized beds (FB), drop tube reactors (DTR), heated grid (HGR) or heated strip reactors (HSR). Combustion of the torrefied biomass or char is investigated in a second stage (*pathC*) by TGA and the experimental matrix of the combustion tests, in this case, can consist of either non-isothermal tests at different heating rates (*pathC*.1) or isothermal tests at different temperatures (*pathC*.2).

Mass loss data and their derivatives as a function of time/temperature provide the so called TG and derivative DTG curves.

Combustion indexes (comprehensive combustion performance index, ignition index, burn out index), usable for a preliminary screening of the biomass performance in combustion environments, can be assessed from the DTG peaks of single experiments, according to the definitions reported in the Appendix (Table A.1).

As far as the evaluation of kinetic expressions, the most popular methods rely on multiple tests at different heating rates. These methods, summarised in Table A.2 of the appendix, are the method of Kissinger [66], Friedman [67], Kissinger–Akahira–Sunose [68], Flynn–Wall–Ozawa [69,70], Coats–Redfern [72], Starink [73]. Software packages are indeed able to perform kinetic analysis of TG results by means of the mentioned methods.

2.2. Surveyed papers

Table 2 shows that the vast majority of the surveyed works followed the approach indicated as *pathA* in Fig. 1, in other words they consisted in non-isothermal thermogravimetric experiments on raw biomass in oxidizing atmosphere, most commonly air. Few studies have instead followed the approach indicated as *pathB*, where the combustion runs have been proceeded by a torrefaction or pyrolysis stage. Few recent works, in particular, produced char samples in drop tube reactors or heated strip reactors with CO_2 rich atmospheres, fast heating rates (10000–100000 K/s) and temperature (up to 2000 K) in order to mimic the fast pyrolysis conditions that hold in pulverized oxy combustion boilers [60–65].

2.3. Results reported in the surveyed works

Figs. 2–5 show DTG curves obtained by non-isothermal TGA in air on raw and pre-treated biomass samples. Notably Fig. 2 reports results obtained on raw biomass, i.e. following the experimental approach indicated in Fig. 1 as *pathA*. Instead, Fig. 3 refers to torrefied samples, i.e. to the experimental approach *pathB*.1 + *C*.1, and Figs. 4 and 5 refer to chars prepared under different conditions, i.e. to the experimental approach *pathB*.2 + *C*.1.

When the experimental approach *pathA* of Fig. 1 is followed, the TG curves of biomass generally show two broad ranges of weight loss as temperature is increased above 473 K (exemplary DTG curves in Fig. 2). The first region, in the temperature range (473–673 K circa), corresponds to pyrolysis of the least thermally stable fractions (mainly hemicellulose and cellulose). The second region, in the high temperature rage (T > 673 K) corresponds to char combustion and pyrolysis of the more stable biomass fractions, mainly lignin, whose degradation is known to span over a broad temperature range (433–923 K circa). Mineral matter transformation can also occur in the high temperature

Table 2
Methods and materials used in recently published works on biomass combustion by TGA.

Authors/year of publication	Reference	Samples	Reaction atmosphere	Experimental Method	Corrisponding Path in Fig. 1	Combustion indices	Kinetic analysis method
Álvarez et al. [27]	27	Cellulose; Lignin; Almond shell; Apple tree leaves; Beetroot pellets; Briquette Charcoal; Chestnut tree chips; Cocoa bean husk; Coffee bean husk; Corncob; Eucalyptus tree chips; Extracted olive pomace; Gorse; Grape seed flour; Miscanthus; Olive stone; Olive tree pruning; Pepper plant; Pine and pineapple leave pellets; Pine kernel shell; Pineapple leaf; Rice husk; Sainfoin; Scrubland pruning; Thistle; Vine shoot; Wheat straw; Wheat straw pellets		NI-TGA[1]	*Path A*		CR, FWO, KAS
Buratti et al. [28]	28	Cellulosic ethanol residue		NI-TGA[1]	*Path A*		FWO
Cai et al. (2018)	29	Waste tea; Tea leaves	Oxy[2]	NI-TGA[1]	*Path A*	x	DAEM, FR, FWO
Deng et al. [30]	30	Wheat straw	Oxy[2]	NI-TGA[1]	*Path A*		CR
Garcia-Maraver et al. [31]	31	Agricultural biomass from olive trees (leaves, prunings and wood)		NI-TGA[1]	*Path A*		CR, FR, FWO, KAS
Guizani et al. [32]	32	Olive pomace		NI-TGA[1]	*Path B1 + C1*		Model fitting
Huang et al. [52]	33	Peat		NI-TGA[1]	*Path A*		Model fitting
Islam et al. [34]	34	Karanja (pongamia pinnata) fruit hulls		NI-TGA[1]	*Path B2 + C1*		FWO, KAS
Jayaraman et al. [35]	35	Poplar wood; Halzenut shell		NI-TGA[1]	*Path A*		Arrhenius, CR
Kok et al. (2017)	36	Halzenut shell; Cellulose; Hemicellulose; Lignin		NI-TGA[1]	*Path A*		FWO, KAS
Liang et al. [37]	37	Bamboo; Wood		NI-TGA[1]	*Path A*		CR, FWO
Lopes et al. [38]	38	Guarana seed residue		NI-TGA[1]	*Path A*		CR
López-González et al. [39]	39	Black spruce, Banksiana mixtures, Willow, Common reed, Switchgrass		NI-TGA[1]	*Path A*		CR
Toptas et al. [40]	40	Vine pruning; Olive tree pruning; Corn stalk; Poultry litter		NI-TGA[1]	*Path B1 + C1*		CR
Wang et al. (2018)	41	Pinewood		NI-TGA[1]	*Path A*		FWO
Wilk et al. [42]	42	Pine; Acacia; Miscanthus giganteus		NI-TGA[1]	*Path B1 + C1*		KAS, FWO
[43])	43	Pine wood		NI-TGA[1]	*Path A*	x	CR, FWO, Model fitting, et
Yu et al. [44]	44	Eucalyptus bark		NI-TGA[1]	*Path A*	x	CR, FWO
Liu et al. [45]	45	Switch grass; betroot		NI-TGA[1]	*Path A*		CR, FWO
Zhang et al. [46]	46	Rice husk; Peanut shell; Wheat straw;		NI-TGA[1]	*Path A*	x	CR
Zhang et al. [47]	47	Duckweed		NI-TGA[1]	*Path B1 + C1*	x	FWO
Zhou et al. [48]	48	Soybean stalk; Wheat straw		NI-TGA[1]	*Path A*		integral methods
Zhou et al. [49]	49	Soybean stalk; Sawdust t		NI-TGA[1]	*Path A*		DAEM
Barzegar et al. (2020)	50	Wood chips	Oxy[2]	NI-TGA[1]	*Path B1 + C1*		FWO, KAS, FR
Deng et al. [51]	51	Wheat straw	Oxy[2]	NI-TGA[1]	*Path A*	x	CR
Huang et al. [52]	52	Water hyacinth	Oxy[2]	NI-TGA[1]	*Path A*	x	FWO
Sher et al. [53]	53	Barley straw; Miscanthus; Waste wood; Wheat straw; Willow; Wood pellet	Oxy[2]	NI-TGA[1]	*Path A*		Arrhenius plots
Wu et al. [54]	54	Sedum alfredii Hance		NI-TGA[1]	*Path A*	x	FWO, KAS
Kopczyński et al. [55]	55	Willow		NI-TGA[1], model fitting	*Path B1 + C1*	x	
Hu et al. [56]	56	Bamboo		NI-TGA[1], Staring	*Path B1 + C1*		
Magdziarz et al. [57]	57	Polish wood		NI-TGA[1]	*Path B1 + C1*		KAS, FWO, FR
Li et al. [58]	58	PKS		I-PFR[3]	*Path B1 + C1* *Path B2 + C1*		Model fitting

(*continued on next page*)

Table 2 (*continued*)

Authors/year of publication	Reference	Samples	Reaction atmosphere	Experimental Method	Corrisponding Path in Fig. 1	Combustion indices	Kinetic analysis method
Apicella et al. [59]	50	Cellulose hydrochar		NI-TGA[1]	*Path B2 + C1*		Model fitting
Senneca et al. (2018)	60	Walnut shells		NI-TGA[1]	*Path B2 + C1*		Model fitting
Senneca et al. (2020)	61	Walnut shells		NI-TGA[1]	*Path B2 + C1*		Model fitting
Senneca et al. (2020)	62	Lignin; Cellulose; Hemicellulose		NI-TGA[1]	*Path B2 + C1*		Model fitting
Cerciello et al. [63]	63	Walnut shells		NI-TGA[1]	*Path B2 + C1*		Model fitting
Senneca et al. (2018)	64	Walnut shells		NI-TGA[1]	*Path B2 + C1*		Model fitting
Li et al. [65]	65	Lignin from bagasse and black liquor		NI-TGA[1]	*Path A*	x	

[1] *Non-isothermal Thermogravimetric experiments;* [2]*Oxyfuel atmosphere;* [3]Isothermal Plug Flow Reactor *experiments;* [4]Plug Flow Reactor.

range, such as decomposition of carbonates in calcium rich biomass.

The deconvolution of the DTG curves above 473 K is quite complex and requires the adoption of multiple partly overlapping peaks, as shown in the example of Fig. 5. The readers must be advised against assuming a one to one correspondence between these peaks and peaks of specific biomass components (cellulose, hemicellulose or lignin). In fact, the DTG curves of natural or even synthetic lignocellulosic materials are not the weight sum of the DTG curves obtained for cellulose alone, hemicellulose alone and lignin alone [60,63]: synergistic effects, catalytic active of inorganic matter, effects of extractives etc. do play a role and contribute to the DTG patterns.

Notably thermal degradation in oxidative atmosphere can be enhanced by the concurrent course of purely pyrolytic processes and heterogeneous oxidation. This phenomenon has been investigated for a suite of non-conventional solid fuels, included biomass, by Senneca et al. [74] who used the term *"oxidative pyrolysis"* to distinguish it from the purely thermally activated degradation reactions typical of inert pyrolysis.

When torrefaction treatments are carried out prior to oxidation [32,40,42,47,55–58], according to the methodological approach described as *pathB*.1 + *C*.1, during the combustion tests (*C*.1) the early mass loss events decrease, as a consequence of the fact that the less thermally stable fractions are partly lost in the pretreatment, as can be observed in the example reported in Fig. 3. When the severity of biomass pretreatment (temperature and time of heating) increases, the early mass loss stages are progressively reduced, this can be clearly observed in Fig. 4, reporting the combustion DTG curves of biomass char samples produced under different conditions in a drop tube reactor (*pathB*.2 + *C*.1).

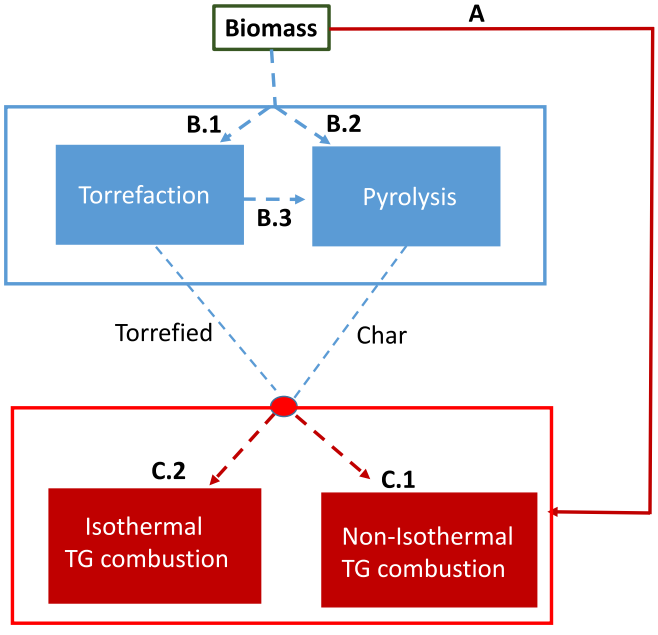

Fig. 1. Experimental approach and methodology for kinetic analysis.

Some of the references works evaluated the TGA data in order to obtain combustion indexes, according to the methods reported in the Appendix.

As far as the results of kinetic analysis is concerned, notably most of the works applied *iso*-conversional methods, in particular those of Kissinger–Akahira–Sunose (KAS) [68], Flynn–Wall–Ozawa (FWO) [69–70], Coats–Redfern (CR) [72]. These methods are often implemented in software packages for thermogravimetric analysis. Few works employed parallel reaction and model fitting methods [32,33,43,58–63].

The kinetic parameters obtained in the references works are reported in Table 3. The comparison of the activation energy values reported in the referenced literature show large variations among research groups, for a given research group among different materials and for a given material at different conversion degree α. Altogether, activation energy values span from 10 to 250 kJ/mol.

The pre-combustion treatments also affect the values of activation energy. Magdziarz et al. [57], Wilk et al. [42] and Hu et al. [56] found that torrefaction decreased the measured values of activation energy for the combustion process, while Kopczyński, et al. [55] found that the activation energy of the second stage (combustion) decreased, conversely that of the first stage (pyrolysis) increased with increasing torrefaction temperature.

In Fig. 4, it is possible to observe also the differences between samples produced in N_2 and CO_2 atmospheres. The presence of CO_2 during in the early stages of pyrolysis in a DTR (0.1 s circa) results in chars with a low share of components with early DTG combustion peaks, however for longer residence times in the DTR the differences between chars produced in N_2 and CO_2 atmosphere become negligible. A larger array of experiments according to the methodological path indicated as *pathB*.2 +*C*.2 in Fig. 1 are reported in refs [59–64] and confirms that CO_2 rich atmospheres, typical of oxy combustion, can accelerate the degradation of selected biomass components over exposure times much shorter than the times of heterogeneous carbon gasification.

The biomass combustion rate in CO_2 rich atmosphere throughout non-isothermal oxy combustion has been investigated in some of the referenced works [29,30,50–53] and the main result is that the qualitative patterns of DTG curves is not dramatically changed, but the values of activation energy in the combustion stage are lower.

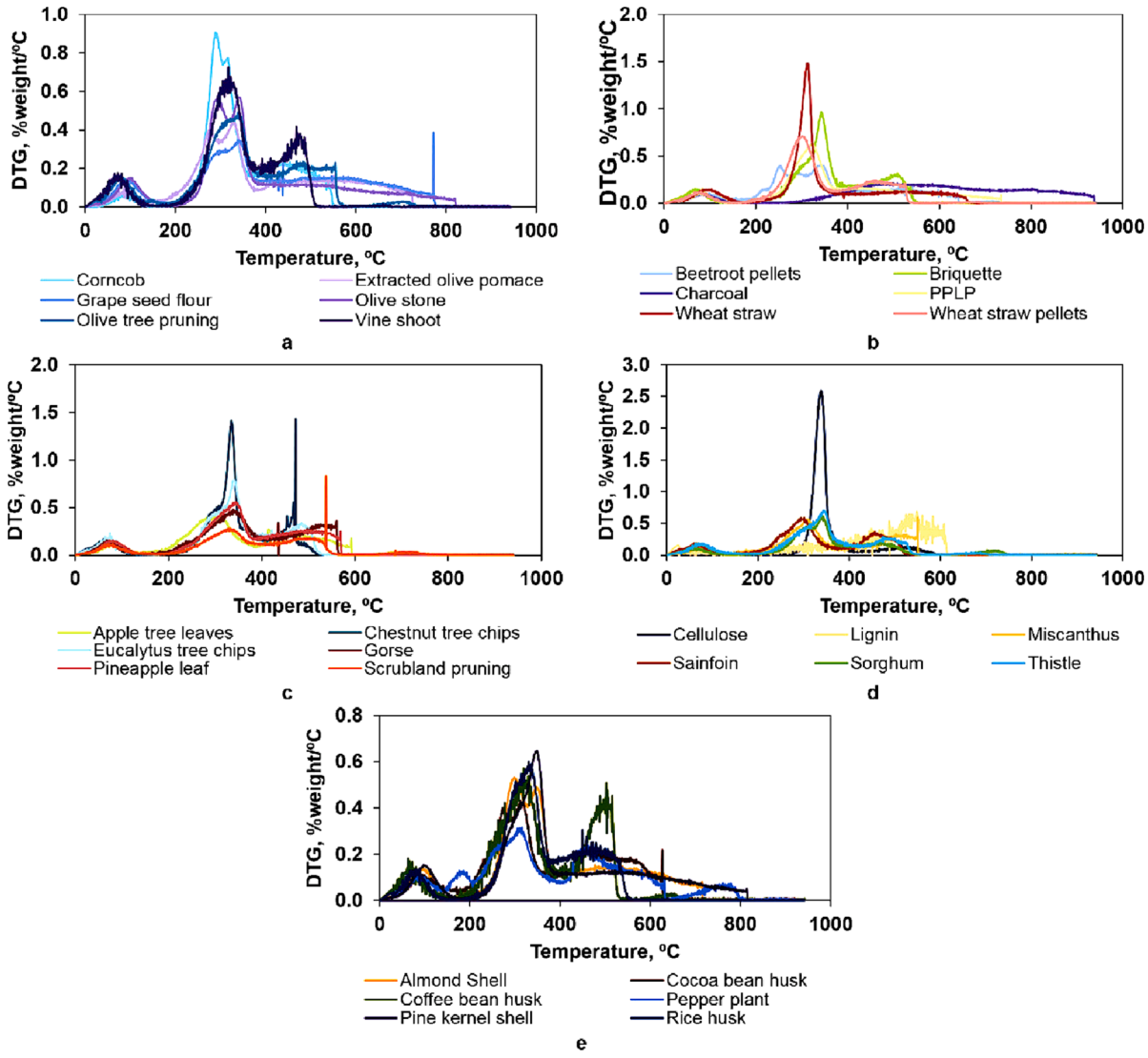

Fig. 2. DTG curves of the combustion process of raw biomass samples (*pathA* of Fig. 1). From [27], Copyright 2016, with permission of Elsevier.

3. Criticalities and limits of the surveyed works and conventional kinetic approach

The kinetic parameters obtained in the surveyed references for different biomass types have been summarized in Table 3 and used to draw Arrhenius plots of the combustion rate. Arrhenius plots obtained with all the data available are shown in Fig. 6A. It can be seen that the wide variability in reported kinetic parameters reflects in combustion rates which differ by order of magnitude especially at realistic boilers temperatures.

Of course the various referenced work refer to different biomass and used different analytical methods for the estimation of kinetic parameters, therefore in Fig. 6B the comparison has been limited to biomass of similar nature, in particular woody biomass, and to the same type of kinetic analysis, in particular the Coat-Redfern method (CR).

Even when the analysis is restricted to similar bimass type and analythical methods, as in the exemplary plots of Fig. 6B, differences in combustion rate remain very significant. It is worth noticing that discrepancies are larger the further away from the temperature range of thermogravimetric experiments, indeed around 700 K the ratio between the highest and the lowest predicted rates in Fig. 6B is approximately 50, but at 1300 K it exceeds 100000.

It is evident that it is critical to select a kinetic expression that can predict reliably the intrinsic combustion rate of biomass over a wide range of temperature, and that can be utilized in codes for the simulation of high temperature boilers.

The origin of the large discrepancies in calculated kinetic expressions can be only partly attributed to the methods used to obtain kinetic parameters from TGA data, which have summarized for the readers' convenience in the appendix. In fact a detailed discussion on such methods is beyond the scope of the present work and can be found in refs. [75–77]. What we do want to point out in the present work, instead, is that **no matter which** of the proposed methods of kinetic analysis is used, meaningful results can be obtained only if all of the three following hypothesis are satisfied:

I. inter and intraparticle mass and temperature diffusion resistances are negligible;
II. reactions result in a single stage of mass loss or well-resolved and defined sequential stages;
III. the structure of the solid reactant is relatively constant throughout the experiment.

Fulfilment of condition I can be achieved through careful control of particles size, heating rates and gaseous mass flow. It will not be further discussed in the present work.

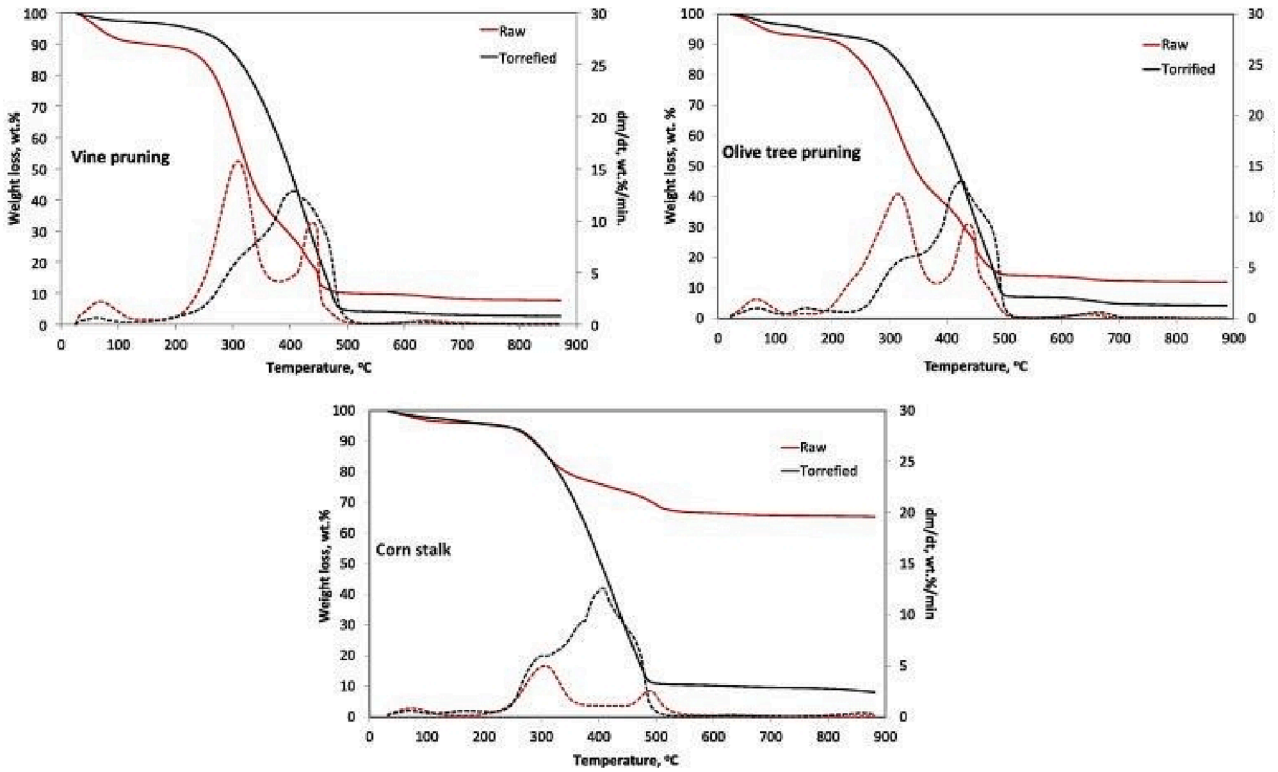

Fig. 3.

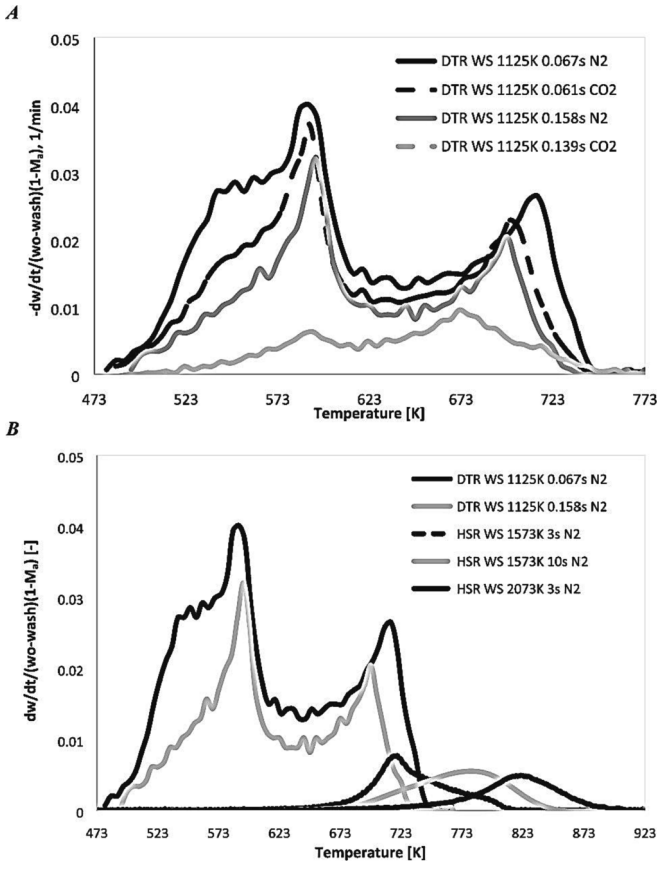

Fig. 4.

Criterion II deserves a more detailed comment, since it is particularly critical for a material like biomass, which is inherently made of several biopolymers of different reactivity. When multiple reaction events are characterized by quite different timescales and the corresponding DTG peaks are well resolved and distant from each other, the values of activation energy obtained at the i^{th} interval of α can be attributed to the i^{th} reaction. Unfortunately, in the case of biomass multiple pyrolysis and combustion reactions occur in parallel and in series and overlap to a good extent. This can determine artefacts and fluctuations in measured values of activation energy [33].

In fact, the mass of sample at any given instant of the non-isothermal combustion experiment is the result of multiple contributions from different components. In the raw biomass, each component is present in its undevolatilized form with weight fraction y_i. Throughout the NI-TG combustion experiment the raw component is transformed into a char component by the pyrolysis reaction i, which is described by a pyrolysis reaction coordinate α_i. Heterogeneous combustion consumes the char generated from pyrolysis of the biomass component i, and the progress of this reaction is described by the reaction coordinate ξ_i.

The overall mass at a given time and the rate of conversion are expressed by Eqs. (1) and (2):

$$\mathrm{m(t)} = \sum_i y_i(m_0(1-\alpha_i) + \alpha_i m_0(1-\xi_i)) \tag{1}$$

$$\frac{d\alpha}{dt} = \sum_i \frac{d\alpha_i}{dt} y_i - \sum_i \frac{d[\alpha_i m_0(1-\xi_i)]}{dt} y_i \tag{2}$$

Notably $\frac{d\alpha}{dt} \neq \sum_i A_i e^{-\frac{Eai}{RT}} f(a_i) y_i$. The kinetic Eq. (A7) (Appendix) is no longer correct because the term $\sum_i \frac{d[\alpha_i m_0(1-\xi_i)]}{dt} y_i$ must also be taken into account. This problem may cause mistakes in the evaluation of kinetic parameters by standard methods which adds onto the kinetic compensation effect between the activation energy and pre-exponential factor, arising from both mathematical and experimental problems [78,79]. Notably, even if an error in the activation energy value can be compensated by the pre-exponential factor in the temperature range of

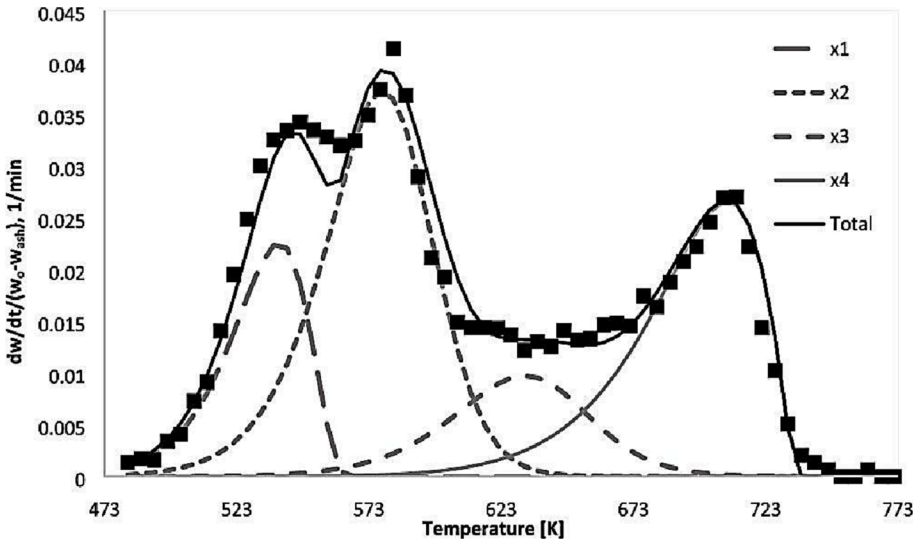

Fig. 5. Example of curve fitting of DTG curves DTG curves of the combustion process of a biomass char samples (walnut shells-WS char prepared in DTR at 950 K in N_2 with short residence time) (*pathB*.2 +*C*.1 of Fig. 1). Reprinted with permission from [61], Copyright 2020, American Chemical Society.

the TG experiments, when the kinetic expression is extrapolated to higher temperature the reaction rates can be seriously under or over predicted.

Criterion III is also critical for biomass because the structure changes progressively along heat treatment, all the way through torrefaction, pyrolysis and char combustion. Under the more severe heating conditions, it has also been shown that the carbonaceous solid structure undergoes structural ordering with increase of aromatic domains at all similar to the phenomenon of thermal annealing of coal [60–63]. Results of experimental work on thermal annealing of lignocellulosic biomass [59–65,74,80] suggested that thermal annealing does not affect in the same way all the biopolymers, but it most likely involves the lignin rich fractions. Moreover, the presence of CO_2 in the atmosphere, as in oxy-combustion, enhances structural rearrangement and thermal annealing [60,61].

It can be concluded, that conditions II and III are not fulfilled for biomass, therefore validity of kinetic expressions obtained by the popular NI-TGA approaches must be carefully considered, especially if the kinetic equations must be implemented in comprehensive models of boilers operating at high heating rate and temperatures.

4. Alternative metod for derivation of biomass kinetic expression suitable for boilers simulation

Predicting the combustion behavior of biomass in real systems of course implies coupling thermo-fluid dynamic models with appropriate single particle reaction models. Recent work emphasised the need to investigate and implement in single particle models also the mutual interactions between thermochemical processes and particle size, aspect ratio, morphology and porosity. All these aspects have the potential to impact severily on the combustion performances of real boilers [81–87] and certainly need to be investigated in the future. Besides these considerations, the previous paragraphs have shown the difficulty to obtain reliable kinetic rate expressions from conventional TGA approaches.

In the present work, an alternative methodology has been applied to select suitable kinetic expressions for combustion of Walnut Shells (WS) under industrial conditions. Notably these describe only intrinsic kinetics which should further be corrected for mass transfer effects in a combustor model.

The experimental approach followed the path indicated in Fig. 1 as *pathB*.2 + *C*1. Samples were pyrolysed (*pathB*.2) in a DTR in Bochum under inert conditions at T = 1273 K and with residence times between 66 and 115 ms, then the combustion rate of chars was investigated by NI-TGA in air (*pathC*.1) in Naples [64]. The surprising result was that the DTG combustion curves of the different DTR-chars exhibited up to four peaks (see Fig. 5). The four components, hereby called C_1, C_2, C_3, C_4, were present in different percentages in the char samples produced with different residence time/temperature.

As already said in previous paragraphs, it would be unrigorous and purely speculative to identify C1, C2, C3, and C4 with the different biopolymers present in lignocellulosic biomass (namely cellulose, lignin etc.). It can be suggested, instead, that C1, C2 are components with relatively “fresh” carbon material (they have not yet evolved in char and even include residues of un-devolatilized matter); C3 and C4 can be considered char materials (with no residual volatile matter) with different degrees of structural organization.

Kissinger methods were applied to each of the four DTG peaks in order to obtain first tentative values of the kinetic parameters for each of the four components, assuming a first order power law. The kinetic parameters were further refined applying a curve fitting procedure to the overall DTG curves [64]. These kinetic expressions have been used to calculate the rate of combustion of each component as a function of temperature in air, and results are reported in the form of Arrhenius plots in Fig. 7A. Two curves have been drawn in Fig. 7B which describe the rate of combustion of the most and least reactive char component as a function of temperature. Fig. 7C shows that these two curves fall in the middle of the cloud of Arrhenius plots obtained with the kinetic parameters reported in the previously surveyed papers.

It can be observed that a T < 700 K the component C_1 burns first, followed by C_2, C_3 and C_4. In this temperature range, combustion is therefore lead by C_1 whereas C_4 may determine combustion tails. This means that, within a first approximation, the accuracy of the rate of C4 determines the capacity of the model to capture temperature peak profiles in the burner. The rate of C1 would instead determine the capacity of the model to describe combustion tails and, ultimately, the level of unburnbed carbon. At temperatures between 700 and 1400 K the situation is different, indeed components C_2 is fastest. Above 1400 K, combustion is led by the fourth component, C_4.

Table 3
Biomass combustion kinetic parameters by TGA.

Ref	Sample	Kinetic method	Atmosphere (if different from air)	Range of conversion (alfa) or temperature interval	E_a kJ/mol	A 1/min
27	Lignin	CR			$6.95{\cdot}10^{1}$	$6.87{\cdot}10^{3}$
27	Almond shell	CR			$1.71{\cdot}10^{1}$	$1.00{\cdot}10^{0}$
27	Apple tree leaves	CR			$2.06{\cdot}10^{1}$	$2.65{\cdot}10^{0}$
27	Beetroot pellets	CR			$2.32{\cdot}10^{1}$	$3.99{\cdot}10^{0}$
27	Briquette	CR			$5.55{\cdot}10^{1}$	$2.24{\cdot}10^{3}$
27	Chestnut tree chips	CR			$5.38{\cdot}10^{1}$	$2.83{\cdot}10^{3}$
27	Cocoa bean husk	CR			$1.51{\cdot}10^{1}$	$6.28{\cdot}10^{-1}$
27	Coffee bean husk	CR			$6.25{\cdot}10^{1}$	$7.10{\cdot}10^{3}$
27	Corncob	CR			$1.95{\cdot}10^{1}$	$3.20{\cdot}10^{0}$
27	Eucalyptus tree chips	CR			$6.30{\cdot}10^{1}$	$1.03{\cdot}10^{4}$
27	Extracted olive pomac	CR			$1.46{\cdot}10^{1}$	$5.08{\cdot}10^{-1}$
27	Gorse	CR			$4.71{\cdot}10^{1}$	$3.31{\cdot}10^{2}$
27	Grape seed flour	CR			$5.70{\cdot}10^{1}$	$3.09{\cdot}10^{2}$
27	Miscanthus	CR			$5.09{\cdot}10^{1}$	$6.76{\cdot}10^{2}$
27	Olive stone	CR			$4.76{\cdot}10^{1}$	$7.33{\cdot}10^{1}$
27	Olive tree pruning	CR			$1.92{\cdot}10^{1}$	$2.26{\cdot}10^{0}$
27	Pepper plant	CR			$4.73{\cdot}10^{1}$	$7.02{\cdot}10^{1}$
27	Pine and pineapple leave pellets	CR			$7.35{\cdot}10^{1}$	$1.01{\cdot}10^{-1}$
27	Pine kernel shell	CR			$4.81{\cdot}10^{1}$	$7.91{\cdot}10^{1}$
27	Pineapple leaf	CR			$4.92{\cdot}10^{1}$	$5.33{\cdot}10^{2}$
27	Rice husk	CR			$3.28{\cdot}10^{1}$	$4.13{\cdot}10^{1}$
27	Sainfoin	CR			$4.09{\cdot}10^{1}$	$1.88{\cdot}10^{2}$
27	Scrubland pruning	CR			$2.09{\cdot}10^{1}$	$2.86{\cdot}10^{0}$
27	Sorghum	CR			$1.81{\cdot}10^{1}$	$2.01{\cdot}10^{0}$
27	Thistle	CR			$3.05{\cdot}10^{1}$	$5.61{\cdot}10^{1}$
27	Vine shoot	CR			$4.82{\cdot}10^{1}$	$8.68{\cdot}10^{2}$
27	Wheat straw	CR			$2.34{\cdot}10^{1}$	$4.13{\cdot}10^{0}$
27	Wheat straw pellets	CR			$2.75{\cdot}10^{1}$	$1.51{\cdot}10^{1}$
28	Cellulose	FWO		alfa = 0.5	$8.04{\cdot}10^{1}$	n.a.
29	Waste tea	FRIEDMAN		alfa = 0.5	$2.45{\cdot}10^{2}$	n.a.
29	Waste tea	FWO		alfa = 0.5	$2.27{\cdot}10^{2}$	n.a.
29	Waste tea	DEAM		alfa = 0.5	$2.29{\cdot}10^{2}$	n.a.
29	Waste tea	FRIEDMAN	80 %CO_2 20 %O_2	alfa = 0.5	$2.05{\cdot}10^{2}$	n.a.
29	Waste tea	FWO	80 %CO_2 20 %O_2	alfa = 0.5	$2.01{\cdot}10^{2}$	n.a.
29	Waste tea	DEAM	80 %CO_2 20 %O_2	alfa = 0.5	$2.02{\cdot}10^{2}$	n.a.
29	Tea leaves	FRIEDMAN		alfa = 0.5	$1.92{\cdot}10^{2}$	n.a.
29	Tea leaves	FWO		alfa = 0.5	$2.29{\cdot}10^{2}$	n.a.
29	Tea leaves	DEAM		alfa = 0.5	$2.30{\cdot}10^{2}$	n.a.
29	Tea leaves	FRIEDMAN	80 %CO_2 20 %O_2	alfa = 0.5	$1.64{\cdot}10^{2}$	n.a.
29	Tea leaves	FWO	80 %CO_2 20 %O_2	alfa = 0.5	$1.93{\cdot}10^{2}$	n.a.
29	Tea leaves	DEAM	80 %CO_2 20 %O_2	alfa = 0.5	$1.94{\cdot}10^{2}$	n.a.
30	Straw	CR			$1.16{\cdot}10^{2}$	$7.50{\cdot}10^{8}$
30	Straw	CR	80 %CO_2 20 %O_2		$1.71{\cdot}10^{2}$	$1.07{\cdot}10^{9}$
31	Leaves	KAS		T > 673 K	$1.14{\cdot}10^{2}$	$6.70{\cdot}10^{27}$
31	Leaves	FWO		T > 673 K	$1.16{\cdot}10^{2}$	$1.10{\cdot}10^{25}$
31	Leaves	FRIEDMAN		T > 673 K	$8.91{\cdot}10^{1}$	$3.70{\cdot}10^{16}$
31	Leaves	CR		T > 673 K Hr = 10 K/min	$8.90{\cdot}10^{1}$	$4.58{\cdot}10^{-1}$
31	Prunings	KAS		T > 673 K	$1.05{\cdot}10^{2}$	$1.20{\cdot}10^{35}$
31	Prunings	FWO		T > 673 K	$1.07{\cdot}10^{2}$	$1.40{\cdot}10^{32}$
31	Prunings	CR		T > 673 K Hr = 10 K/min	$8.75{\cdot}10^{1}$	$1.91{\cdot}10^{10}$
31	Prunings	FRIEDMAN		T > 673 K	$4.99{\cdot}10^{1}$	$1.00{\cdot}10^{15}$
31	Wood	KAS		T > 673 K	$8.10{\cdot}10^{1}$	$3.40{\cdot}10^{31}$
31	Wood	FWO		T > 673 K	$8.48{\cdot}10^{1}$	$4.50{\cdot}10^{28}$
31	Wood	FRIEDMAN		T > 673 K	$1.09{\cdot}10^{1}$	$6.90{\cdot}10^{2}$
31	Wood	CR		T > 673 K Hr = 10 K/min	$7.39{\cdot}10^{1}$	$1.15{\cdot}10^{17}$
32	Olive pomace	MODEL FITTING			$1.50{\cdot}10^{2}$	$2.39{\cdot}10^{12}$
32	Olive pomace torrefied 503 K	MODEL FITTING			$1.50{\cdot}10^{2}$	$6{\cdot}10^{10}$
32	Olive pomace torrefied 523 K	MODEL FITTING			$1.50{\cdot}10^{2}$	$1.51{\cdot}10^{11}$
32	Olive pomace torrefied 543 K	MODEL FITTING			$1.50{\cdot}10^{2}$	$1.9{\cdot}10^{11}$
32	Olive pomace torrefied 563 K	MODEL FITTING	air		$1.50{\cdot}10^{2}$	$3.01{\cdot}10^{11}$
32	Olive pomace torrefied 583 K	MODEL FITTING			$1.50{\cdot}10^{2}$	$1.9{\cdot}10^{11}$
34	Karania	KAS		alfa = 0.5	$5.20{\cdot}10^{1}$	$1.03{\cdot}10^{2}$
34	Karania	FWO		alfa = 0.5	$6.30{\cdot}10^{1}$	$2.33{\cdot}10^{3}$
35	Poplar wood	ARRHENIUS			$5.09{\cdot}10^{2}$	$3.96{\cdot}10^{2}$
35	Poplar wood	CR			$7.50{\cdot}10^{1}$	$1.97{\cdot}10^{5}$
35	Hezelnut shells	ARRHENIUS			$1.05{\cdot}10^{2}$	$2.51{\cdot}10^{10}$
35	Hezelnut shells	CR			$8.10{\cdot}10^{1}$	$1.40{\cdot}10^{5}$
36	Hezelnut shells	KAS		average	$8.38{\cdot}10^{1}$	n.a.
36	Cellulose	KAS		average	$1.49{\cdot}10^{2}$	n.a.
36	Hemicellulose	KAS		average	$1.37{\cdot}10^{2}$	n.a.

(*continued on next page*)

Table 3 (*continued*)

Ref	Sample	Kinetic method	Atmosphere (if different from air)	Range of conversion (alfa) or temperature interval	E_a kJ/mol	A 1/min
36	Lignin	KAS		average	$1.41 \cdot 10^{2}$	n.a.
36	Hezelnut shells	FWO		average	$9.33 \cdot 10^{1}$	n.a.
36	Cellulose	FWO		average	$1.90 \cdot 10^{2}$	n.a.
36	Hemicellulose	FWO		average	$1.79 \cdot 10^{2}$	n.a.
36	Lignin	FWO		average	$1.91 \cdot 10^{2}$	n.a.
37	Bamboo/ wood	CR		Hr = 20 K/min	$1.32 \cdot 10^{2}$	$1.46 \cdot 10^{9}$
37	Bamboo/ wood			Hr = 30 K/min	$1.26 \cdot 10^{2}$	$8.35 \cdot 10^{8}$
37	Bamboo/ wood			Hr = 40 K/min	$1.44 \cdot 10^{2}$	$2.00 \cdot 10^{10}$
38	Agroindustrial residue				$7.80 \cdot 10^{1}$	$5.92 \cdot 10^{3}$
39	Reed phalaris	CR			$9.80 \cdot 10^{1}$	$6.50 \cdot 10^{6}$
39	Switchgrass	CR			$8.30 \cdot 10^{1}$	$7.90 \cdot 10^{5}$
39	Common reed	CR			$6.70 \cdot 10^{1}$	$5.80 \cdot 10^{4}$
39	Black spruce	CR			$1.12 \cdot 10^{2}$	$9.80 \cdot 10^{7}$
39	Pinus banksiana	CR			$1.43 \cdot 10^{2}$	$2.70 \cdot 10^{10}$
40	Corn stalk	CR		719 K < T < 829 K	$1.68 \cdot 10^{2}$	$7.36 \cdot 10^{17}$
40	Olive tree pruning	CR		650 K < T < 785 K	$4.82 \cdot 10^{1}$	$1.11 \cdot 10^{2}$
40	Vine pruning	CR		381 °C < T < 521 °C	$4.51 \cdot 10^{1}$	$7.90 \cdot 10^{1}$
40	Corn stalk torrefied	CR		211 °C < T < 521 °C	$7.55 \cdot 10^{1}$	$3.53 \cdot 10^{3}$
40	Olive tree pruning torrefied	CR		237 °C < T < 517 °C	$5.89 \cdot 10^{1}$	$1.12 \cdot 10^{3}$
40	Vine pruning torrefied	CR		181 °C < T < 521 °C	$5.17 \cdot 10^{2}$	$2.47 \cdot 10^{2}$
41	Pine wood	FWO			$1.82 \cdot 10^{2}$	n.a.
42	Acacia	KAS		alfa = 0.5	$2.13 \cdot 10^{2}$	$1.88 \cdot 10^{10}$
42	Acacia torrefied	KAS		alfa = 0.5	$9.87 \cdot 10^{1}$	$1.13 \cdot 10^{0}$
42	Pine	KAS		alfa = 0.5	$1.32 \cdot 10^{2}$	$7.04 \cdot 10^{4}$
42	Pine torrefied	KAS		alfa = 0.5	$9.18 \cdot 10^{1}$	$2.71 \cdot 10^{1}$
42	Mischantus	KAS		alfa = 0.5	$2.16 \cdot 10^{2}$	$7.53 \cdot 10^{9}$
42	Miscantus torrefied	KAS		alfa = 0.5	$1.28 \cdot 10^{2}$	$1.75 \cdot 10^{2}$
42	Acacia	OFW		alfa = 0.5	$2.29 \cdot 10^{2}$	$4.24 \cdot 10^{19}$
42	Acacia torrefied	OFW		alfa = 0.5	$1.18 \cdot 10^{2}$	$3.79 \cdot 10^{9}$
42	Pine	OFW		alfa = 0.5	$1.79 \cdot 10^{2}$	$6.73 \cdot 10^{14}$
42	Pine torrefied	OFW		alfa = 0.5	$1.07 \cdot 10^{2}$	$3.30 \cdot 10^{8}$
42	Mischantus	OFW		alfa = 0.5	$2.20 \cdot 10^{2}$	$1.20 \cdot 10^{19}$
42	Miscantus torrefied	OFW		alfa = 0.5	$1.57 \cdot 10^{2}$	$1.89 \cdot 10^{13}$
43	Pinewood	OFW, DAEM STARINK		average	$1.86 \cdot 10^{2}$	$1.66 \cdot 10^{3}$
44	Eucalyptus bark	CR		Hr = 10 K/min	$2.78 \cdot 10^{1}$	$4.49 \cdot 10^{3}$
44	Eucalyptus bark	CR		Hr = 15 K/min	$5.97 \cdot 10^{1}$	$2.44 \cdot 10^{5}$
44	Eucalyptus bark	CR		Hr = 20 K/min	$1.01 \cdot 10^{2}$	$2.84 \cdot 10^{9}$
45	Beetroot	CR		Hr = 10 K/min	$5.01 \cdot 10^{1}$	$2.33 \cdot 10^{3}$
45	Beetroot	CR		Hr = 30 K/min	$4.34 \cdot 10^{1}$	$1.22 \cdot 10^{3}$
45	Beetroot	CR		Hr = 50 K/min	$4.31 \cdot 10^{1}$	$1.80 \cdot 10^{3}$
45	Beetroot	CR		Hr = 70 K/min	$3.81 \cdot 10^{1}$	$8.64 \cdot 10^{2}$
45	Beetroot	CR		Hr = 90 K/min	$4.18 \cdot 10^{1}$	$2.87 \cdot 10^{2}$
45	Switchgrass	CR		Hr = 10 K/min	$7.14 \cdot 10^{1}$	$3.24 \cdot 10^{5}$
45	Switchgrass	CR		Hr = 30 K/min	$8.13 \cdot 10^{1}$	$4.18 \cdot 10^{6}$
45	Switchgrass	CR		Hr = 50 K/min	$6.94 \cdot 10^{1}$	$5.81 \cdot 10^{5}$
45	Switchgrass	CR		Hr = 70 K/min	$5.89 \cdot 10^{1}$	$9.06 \cdot 10^{4}$
45	Switchgrass	CR		Hr = 90 K/min	$5.56 \cdot 10^{1}$	$6.90 \cdot 10^{4}$
46	Peanut shell			708 K < T < 890 K	$2.58 \cdot 10^{2}$	$2.77 \cdot 10^{16}$
47	Duckweed	DOYLE MODEL		663 K < T < 753 K	$1.68 \cdot 10^{1}$	$5.03 \cdot 10^{1}$
47	Duckweed wet torreffaction 403 K	DOYLE MODEL		663 K < T < 753 K	$2.40 \cdot 10^{1}$	$1.13 \cdot 10^{2}$
47	Duckweed wet torreffaction 433 K	DOYLE MODEL		633 K < T < 753 K	$3.18 \cdot 10^{1}$	$4.02 \cdot 10^{2}$
47	Duckweed wet torreffaction 463 K	DOYLE MODEL		623 K < T < 743 K	$4.24 \cdot 10^{1}$	$2.49 \cdot 10^{3}$
47	Duckweed wet torreffaction 493 K	DOYLE MODEL		623 K < T < 743 K	$4.35 \cdot 10^{1}$	$2.70 \cdot 10^{3}$
47	Duckweed wet torreffaction 523 K	DOYLE MODEL		623 K < T < 743 K	$5.22 \cdot 10^{1}$	$1.16 \cdot 10^{4}$
48–49	Soybean stalk	INTEGRAL		663 K < T < 786 K	$5.25 \cdot 10^{1}$	n.a.
48–49	Wheat straw	INTEGRAL		700 K < T < 812 K	$5.39 \cdot 10^{1}$	n.a.
50	Pinewood	FWO			$1.75 \cdot 10^{2}$	Min: $5.43 \cdot 10^{6}$
50	Pinewood	KAS			$1.73 \cdot 10^{2}$	Max:
50	Pinewood	FRIEDMAN			$1.65 \cdot 10^{2}$	$1.64 \cdot 10^{16}$
50	Pinewood	FWO	80 %CO_2 20 %O_2		$1.86 \cdot 10^{2}$	Min: $9.68 \cdot 10^{7}$
50	Pinewood	KAS	80 %CO_2 20 %O_2		$1.85 \cdot 10^{2}$	Max:
50	Pinewood	FRIEDMAN	80 %CO_2 20 %O_2		$1.77 \cdot 10^{2}$	$1.58 \cdot 10^{17}$
50	Pinewood torrefied 623 K	FWO			$1.01 \cdot 10^{2}$	Min: $2.98 \cdot 10^{3}$
50	Pinewood torrefied 623 K	KAS			$9.28 \cdot 10^{1}$	Max:
50	Pinewood torrefied 623 K	FRIEDMAN			$5.72 \cdot 10^{1}$	$1.08 \cdot 10^{15}$
50	Pinewood torrefied 623 K	FWO	80 %CO_2 20 %O_2		$9.44 \cdot 10^{1}$	Min: $2.88 \cdot 10^{3}$
50	Pinewood torrefied 623 K	KAS	80 %CO_2 20 %O_2		$8.59 \cdot 10^{1}$	Max:
50	Pinewood torrefied 623 K	FRIEDMAN	80 %CO_2 20 %O_2		$5.23 \cdot 10^{1}$	$1.95 \cdot 10^{13}$
51	Wheat straw	CR			$1.42 \cdot 10^{1}$	$1.43 \cdot 10^{0}$

(*continued on next page*)

Table 3 (*continued*)

Ref	Sample	Kinetic method	Atmosphere (if different from air)	Range of conversion (alfa) or temperature interval	E_a kJ/mol	A 1/min
51	Wheat straw	CR	80 %CO_2 20 %O_2		$1.46{\cdot}10^{1}$	$1.44{\cdot}10^{0}$
51	Wheat straw	CR	70 %CO_2 30 %O_2		$1.30{\cdot}10^{1}$	$1.04{\cdot}10^{0}$
51	Wheat straw	CR	65 %CO_2 35 %O_2		$1.74{\cdot}10^{1}$	$3.35{\cdot}10^{0}$
52	Sewage sludge	FWO	80 %CO_2 20 %O_2		$1.64{\cdot}10^{2}$	$1.82{\cdot}10^{16}$
52	Sewage sludge	FWO	70 %CO_2 30 %O_2		$1.16{\cdot}10^{2}$	$2.27{\cdot}10^{11}$
52	Sewage sludge	FWO	50 %CO_2 50 %O_2		$1.65{\cdot}10^{2}$	$4.07{\cdot}10^{16}$
52	Sewage sludge	FWO	30 %CO_2 70 %O_2		$2.30{\cdot}10^{2}$	$1.41{\cdot}10^{23}$
53	Barley straw	ARRHENIUS			$3.80{\cdot}10^{2}$	n.a.
53	Miscanthus	ARRHENIUS			$3.04{\cdot}10^{2}$	n.a.
53	Waste wood	ARRHENIUS			$1.98{\cdot}10^{2}$	n.a.
53	Wheat straw	ARRHENIUS			$1.68{\cdot}10^{2}$	n.a.
53	Willow	ARRHENIUS			$1.70{\cdot}10^{2}$	n.a.
53	Wood pellet	ARRHENIUS			$1.99{\cdot}10^{2}$	n.a.
53	Barley straw	ARRHENIUS	70 %CO_2 30 %O_2		$1.94{\cdot}10^{2}$	n.a.
53	Miscanthus	ARRHENIUS	70 %CO_2 30 %O_2		$2.27{\cdot}10^{2}$	n.a.
53	Waste wood	ARRHENIUS	70 %CO_2 30 %O_2		$3.40{\cdot}10^{2}$	n.a.
53	Wheat straw	ARRHENIUS	70 %CO_2 30 %O_2		$3.04{\cdot}10^{2}$	n.a.
53	Willow	ARRHENIUS	70 %CO_2 30 %O_2		$3.33{\cdot}10^{2}$	n.a.
53	Wood pellet	ARRHENIUS	70 %CO_2 30 %O_2		$4.17{\cdot}10^{2}$	n.a.
55	Willow				$1.46{\cdot}10^{2}$	$9.00{\cdot}10^{10}$
55	Willow torrefied 473 K				$1.41{\cdot}10^{2}$	$1.38{\cdot}10^{10}$
55	Willow torrefied 493 K				$1.16{\cdot}10^{2}$	$2.70{\cdot}10^{8}$
55	Willow torrefied 513 K				$1.13{\cdot}10^{2}$	$1.14{\cdot}10^{8}$
55	Willow torrefied 533 K				$1.09{\cdot}10^{2}$	$5.28{\cdot}10^{7}$
55	Willow torrefied 553 K				$1.38{\cdot}10^{2}$	$1.02{\cdot}10^{10}$
55	Willow torrefied 573 K				$1.36{\cdot}10^{2}$	$5.16{\cdot}10^{9}$
56	Bamboo forest residue			alfa = 0.5	$1.75{\cdot}10^{2}$	$7.02{\cdot}10^{14}$
56	Bamboo forest residue torrefied 473 K			alfa = 0.5	$2.10{\cdot}10^{2}$	$5.21{\cdot}10^{17}$
56	Bamboo forest residue torrefied 523 K			alfa = 0.5	$1.96{\cdot}10^{2}$	$6.90{\cdot}10^{16}$
56	Bamboo forest residue torrefied 573 K			alfa = 0.5	$1.97{\cdot}10^{2}$	$1.97{\cdot}10^{17}$
57	Wood 1	FRIEDMAN			$1.53{\cdot}10^{2}$	$5.64{\cdot}10^{19}$
57	Wood 1	KAS			$1.60{\cdot}10^{2}$	$1.08{\cdot}10^{15}$
57	Wood 1	FWO			$1.62{\cdot}10^{2}$	$1.14{\cdot}10^{15}$
57	Wood 1 torrefied	FRIEDMAN		$1.11{\cdot}10^{2}$	$1.08{\cdot}10^{15}$	
57	Wood 1 torrefied	KAS			$1.05{\cdot}10^{2}$	$4.56{\cdot}10^{11}$
57	Wood 1 torrefied	FWO			$1.10{\cdot}10^{2}$	$8.40{\cdot}10^{11}$
57	Wood 2	FRIEDMAN		$2.32{\cdot}10^{2}$	$5.94{\cdot}10^{20}$	
57	Wood 2	KAS			$2.15{\cdot}10^{2}$	$5.52{\cdot}10^{19}$
57	Wood 2	FWO			$2.15{\cdot}10^{2}$	$3.72{\cdot}10^{19}$
57	Wood 2 torrefied	FRIEDMAN		$1.83{\cdot}10^{2}$	$2.70{\cdot}10^{18}$	
57	Wood 2 torrefied	KAS			$1.88{\cdot}10^{2}$	$9.60{\cdot}10^{15}$
57	Wood 2 torrefied	FWO			$1.89{\cdot}10^{2}$	$9.00{\cdot}10^{15}$
58	Palm kernel shell	MODEL FITTING			$4.75{\cdot}10^{1}$	n.a
58	Palm kernel shell torrefied	MODEL FITTING			$6.00{\cdot}10^{1}$	n.a.
64	Walnut shells char from DTR			Component 1	$5.8{\cdot}10^{1}$	$2.00{\cdot}10^{4}$
64	Walnut shells char from DTR			Component 2	$1.50{\cdot}10^{2}$	$5.00{\cdot}10^{12}$
64	Walnut shells char from DTR			Component 3	$1.50{\cdot}10^{2}$	$3.50{\cdot}10^{11}$
64	Walnut shells char from DTR			Component 4	$2.05{\cdot}10^{2}$	$5.50{\cdot}10^{14}$

With the aim of identifying a simple kinetic expression suitable for reactor models, for instance in CFD (computational fluid dynamics) codes, within a first approximation it is suggested to different sets of kinetic parameters according to the operating reaction temperature, as reported in Table 4.

5. Conclusions

A survey over recent kinetic studies of biomass combustion has shown a very common use of TGA campaigns, especially of non-isothermal experiments (NI-TGA), combined with kinetic analysis methods of Kissinger, Friedman, Kissinger–Akahira–Sunose, Flynn–Wall–Ozawa, Coats–Redfern, Starink.

A critical analysis of these results shows large variability in estimation of biomass combustion rate from TGA derived kinetic expression. Differences cannot be simply attributed to variability of biomass or errors in experimental or data analysis procedures.

Lignocellulosic materials are indeed complex materials where multiple occur in series and parallel. These include the pyrolysis and combustion of different lignocellulosic components as well the progressive transformation of the biomass structure towards the progressively more organized structure of char. Under severe heating conditions, even thermal annealing/graphitization is possible.

TGA is a valuable and easy tool for comparing and scaling the reactivity at the laboratory scale, for instance through combustion indexes, but when multiple stage of mass loss overlap and the structure of the solid reactant is not constant throughout the experiment, as in the case of biomass combustion, thermogravimetric analysis by conventional methids can fail to produce reliable kinetic expressions.

In these cases, sensitive approaches must be developed by expert users to gain insightful results. It is also recommended to pre-pyrolyse the biomass before performing any TG combustion run, in order to

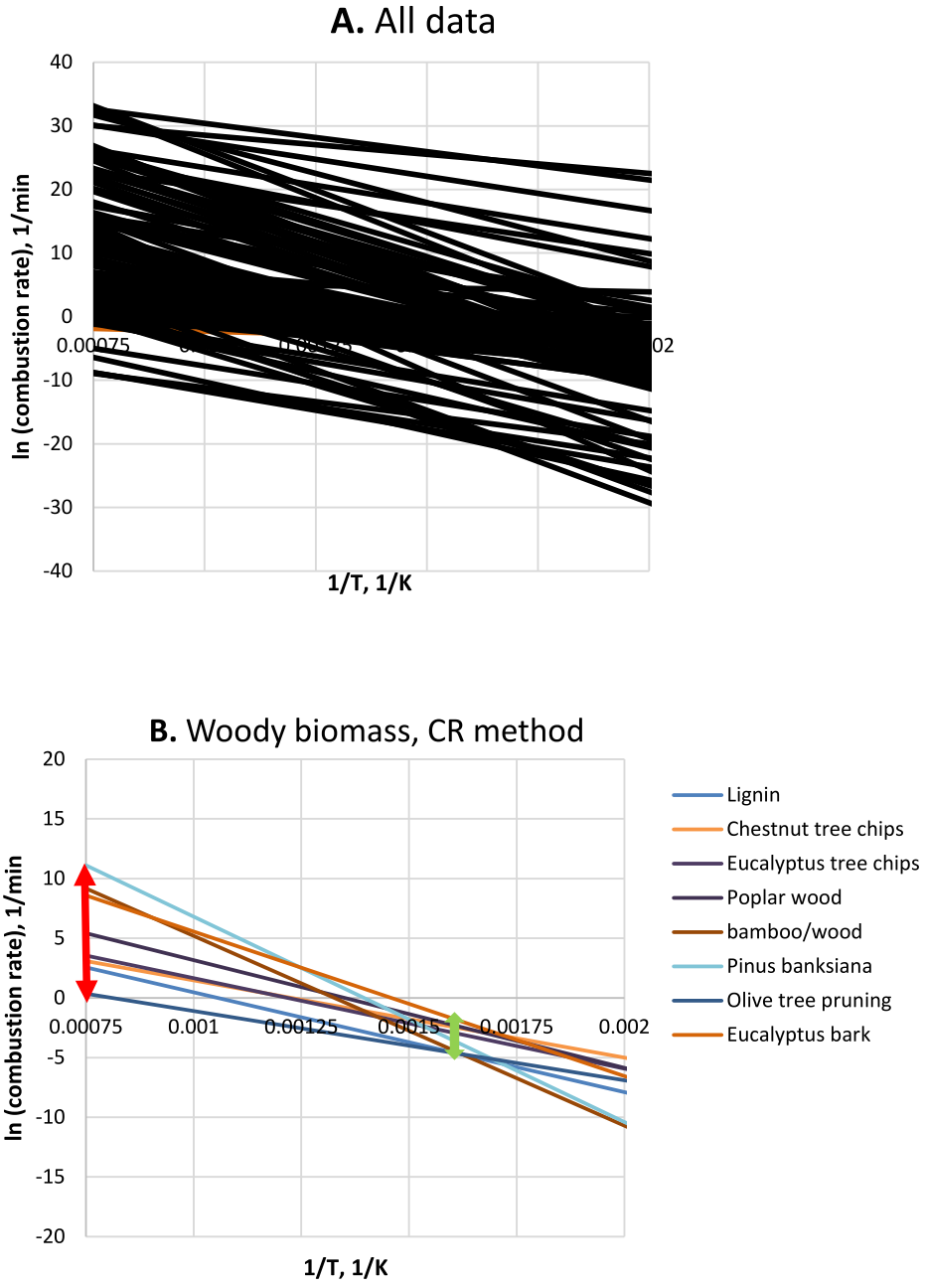

Fig. 6. Arrhenius plots of combustion rate with literature data. A: all data from Table 3; B. woody biomass obtained by CR methods [27,35,37,39,40,44].

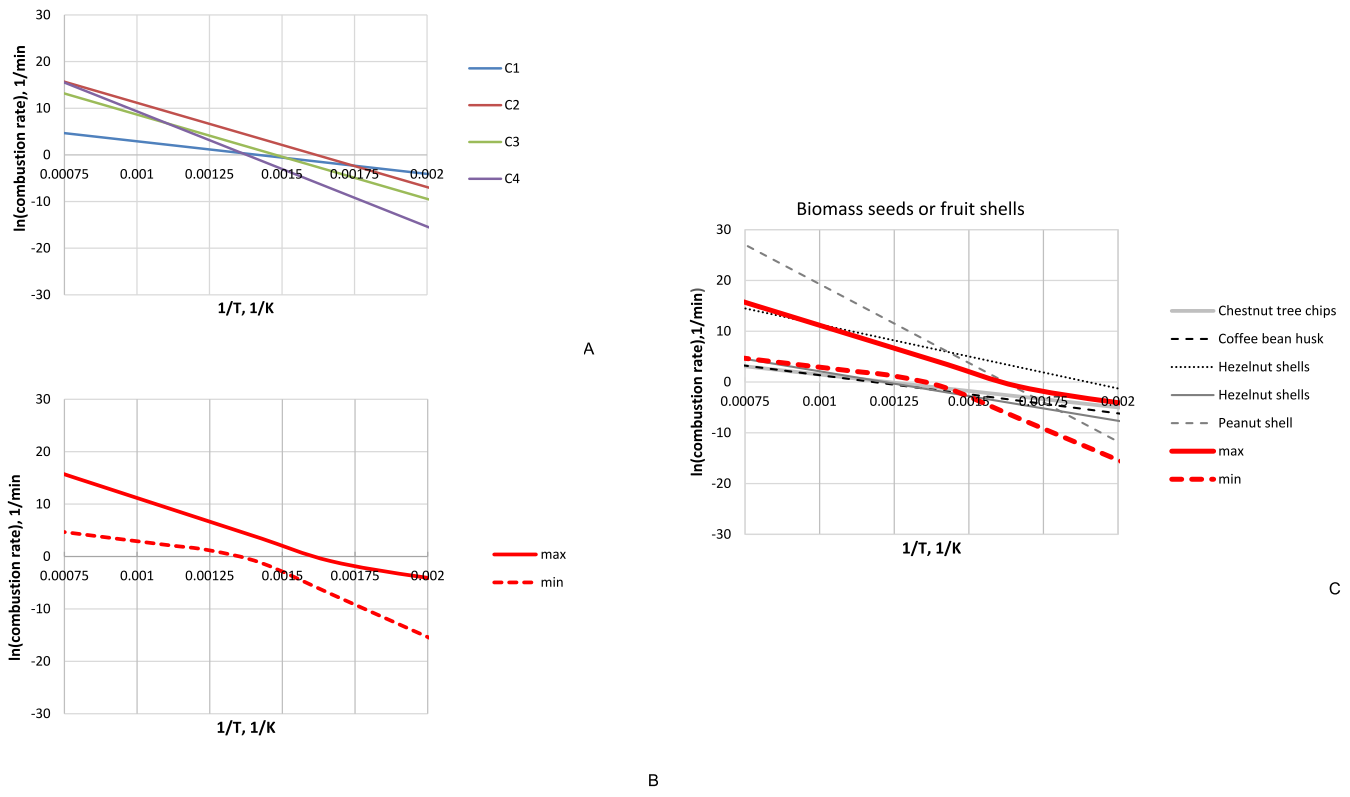

Fig. 7. Arrhenius plots of WS char combustion in air: A. components C_1 – C_4;B: most and least reactive component; C. Comparison with literature results for shells [27,35,36,47].

Table 4

Values of kinetic parameters of WS char combustion in air according to kinetic expression. $\frac{d\alpha}{dt} = k_o e^{-\frac{E_a}{RT}}(1-\alpha)$.

	T < 700 K	1400 > T > 700 K	T > 1400 K
Kinetic-Limited Rate Pre-Exp. Factor, 1/min	$3.3{\cdot}10^{2}$	$8.3{\cdot}10^{10}$	$1.00{\cdot}10^{13}$
Kinetic-Limited Rate Activation Energy, kJ/mol	58	150	205

Table A1
Combustion performance indices.

Performance index	Formula	Meaning
Comprehensive combustion performance index [%2/(°C3 min2)]	$\frac{DTG_{peak}DTG_{av}}{T_i^2 T_b}$	Overall combustion performance
Ignition index [%/min3]	$\frac{DTG_{peak}}{t_i t_{peak}}$	Ignition performance
Burn out index [%/(min)4]	$\frac{DTG_{peak}}{\Delta t_{1/2} t_{peak} t_b}$ $\Delta t_{1/2}$is the time to go from DTG=0.5DTG_{peak} to DTG_{peak}	Burnout performance

limit the structural changes related to pyrolysis and graphitization. Pre-pyrolysis should be carried out with peak temperature, heating rate and residence time as close as possible to realistic conditions.

In the reported exemple of walnut shells combustion, four components have been identified with four distinct sets of kinetic parameters. Within a first order approximation, in a given temperature range, the kinetics of the most reactive component can be used to capture the burnser's temperature peak profiles, however the kinetics of the least reactive component shall be considered to predict combustion tails and, ultimately, the level of unburnbed carbon.

Declaration of Competing Interest

The authors declare the following financial interests/personal relationships which may be considered as potential competing interests: Osvalda Senneca reports financial support was provided by German Research Foundation. Francesca Cerciello reports financial support was provided by German Research Foundation. Osvalda Senneca reports

Table A2
Methods of Kinetic analysis.

Method	Type of method	To be assessed from TG/DTG curves	Plot	Equation
Kissinger [66]	Differential	DTG peak temperature (T_{max}) at different heating rate (β)	$\ln(\beta/T_{max}^2)$vs. $1/T_{max}$	$\ln\left(\frac{\beta}{T_{max}^2}\right) = \ln\left(\frac{AR}{E_a}\right) - \frac{E_a}{RT_{max}}$
Friedman [67]	Differential iso-conversional	Conversion rate ($d\alpha/dt$) and temperature (T_α) at given conversion (α) for different heating rates (β)	$ln(d\alpha/dt)_i$ vs $1/T_\alpha$	$\ln\left(\frac{d\propto}{dt}\right) = \ln[Af(\propto)] - \frac{Ea}{RT}$ For reaction-order nln$\left(\frac{d\propto}{dt}\right)$ = ln(A) + nln(1 −∝) $-\frac{Ea}{RT}$
Kissinger–Akahira–Sunose (KAS) [68]	Integral iso-conversional	Temperature (T_α) at given conversion (α) for different heating rates (β)	$ln(\beta/T_\alpha^2)$ vs. $1/T_\alpha$,	$\ln\left(\frac{\beta}{T_\alpha^2}\right) = \ln\left(\frac{AE_a}{Rg(\alpha)}\right) - \frac{E_a}{RT_\alpha}$ for reaction-order n g(α) = $n^{-1}\cdot(-1+(1-\alpha)^{-n})$
Flynn–Wall–Ozawa (FWO) [69–70]	Integral iso-conversional		$log(\beta)$ vs. $1/T_\alpha$	For n=1 $\log\beta = \log\left(\frac{AE_a}{Rg(\alpha)}\right) - 2.315 - 0.4567\frac{E_a}{RT_\alpha}$ $\ln\beta = \ln\left(\frac{AE_a}{Rg(\alpha)}\right) - 5.332 - 1.052\frac{E_a}{RT_\alpha}$ For reaction order n $\ln(-ln(1-\alpha)) = \ln A - \frac{E_a}{RT_\alpha} - n\ln(\beta)$
DAEM [89]	Integral iso-conversional		$ln(\beta/T_\alpha^2)$ vs. $1/T_\alpha$,	$\ln\left(\frac{\beta}{T_\alpha^2}\right) = \ln\left(\frac{AR}{E_a}\right) + 0.675 - \frac{E_a}{RT_\alpha}$
STARINK [72]	Integral Iso-conversional		$ln(\beta/T_\alpha^{1.92})$ vs. $1/T_\alpha$,	$\ln\left(\frac{\beta}{T_\alpha^{1.92}}\right) = const - 1.00008\frac{E_a}{RT_\alpha}$
Coats–Redfern method [73]	Integral on single heating rate	conversion (α) as a function of temperature at one heating rate	$ln\left(\frac{1-(1-\alpha)^{1-n}}{T^2(1-n)}\right)$	$ln\left(\frac{1-(1-\alpha)^{1-n}}{T^2(1-n)}\right) = \ln\left(\frac{AR}{\beta E_a}\right) - \frac{E_a}{RT}$ (for n≠1);
			or$ln\left(\frac{-\ln(1-\alpha)}{T^2}\right)$ vs. $1/T$	$ln\left(\frac{-\ln(1-\alpha)}{T^2}\right) = \ln\left(\frac{AR}{\beta E_a}\right) - \frac{E_a}{RT}$(for n=1)

financial support was provided by Government of Italy Ministry of Education University and Research.

Data availability

Data will be made available on request.

Acknowledgments

Authors acknowledge funding by Deutsche Forschungsgemeinschaft (DFG, German Research Foundation) – Project-ID 215035359 – TRR 129 Oxyflame. "Gefördert durch die Deutsche Forschungsgemeinschaft (DFG) – Projektnummer 215035359 – TRR 129" and PON BIO-FEEDSTOCK ARS01_00985 (Sviluppo di piattaforme tecnologiche integrate per la valorizzazione di biomasse residuali).

Appendix

A.1 Combustion Performance Indices

Thermogravimetric experiments can be used as a means to obtain a quick comparison of biomass and solid fuels in general in terms of combustion reactivity [88].

From the plots of mass loss (TG curves) and derivative mass loss curves (DTG) versus temperature/time it is possible to identify the ignition and peak temperature and time ($T_i, t_i, T_{peak}, t_{peak}$), the burnout temperature and time (T_b, t_b), the maximum and average of the DTG curves (DTG_{peak}, DTG_{av}).

A first indication on the relative reactivity of samples is provided by simply comparing the peak of the DTG curve: the lower the peak temperature, the more reactive the sample. However different other parameters can be calculated in order to compare the combustion performance of solid fuels. The most commonly used combustion performance indices and their formulas are reported in Table A1.

When comparing combustion indices from different research works it must be born in mind that values depend on the heating program and experimental conditions applied, in particular combustion indices increase with the heating rate.

A.2 Kinetic analysis by TGA

The kinetic analysis from TGA data departs from the general expression:

$$\frac{d\alpha}{dt} = k_o e^{-\frac{E_a}{RT}} f(\alpha) h(p_g) \tag{A1}$$

where k_0 is the pre-exponential factor,E_a the activation energy, T the temperature in K, R the universal gas constant, the functions $f(\alpha)$ and $h(pg)$ describe the dependance of the rate of reaction from the conversion degree (α) and from the reactant gas (oxygen) partial pressure (p_g).

The degree of conversion α is calculated from weight loss data as:

$$\alpha = \frac{w_0 - w_t}{w_0 - w_f} \tag{A2}$$

where w_0 is the initial weight of the sample, w_t is the weight of the sample at a specific time t and w_f the final weight of the sample.

At fixed value of the reactant gas (oxygen) partial pressure in the flow gas, the general conversion-time relationship (A1) simplifies to:

$$\frac{d\alpha}{dt} = Ae^{-\frac{E_a}{RT}}f(\alpha) \tag{A3}$$

The functional form of $f(\alpha)$ is often set to $(1-\alpha)$, however more complex expressions sometimes are used (n' reaction order, nucleation, geometrical contraction models etc.) [27].

Upon heating with constant rate, β, the following relations hold:

$$\frac{d\alpha}{dT} = \frac{A}{\beta}e^{-\frac{E_a}{RT}}f(\alpha) \tag{A4}$$

$$G(\alpha) = \int_0^{\alpha} f(\alpha) = \frac{A}{\beta}\int_{T_0}^{T} e^{\left(-\frac{E_a}{RT}\right)}dT \tag{A5}$$

The kinetic parameters can be obtained applying different methods from isothermal and non-isothermal campaigns.

Isothermal TGA experimental campaigns

For isohtermal thermogravimetric (I-TG) campaigns the function $f(\alpha)$ can be obtained from the shape of the curve of instantaneous conversio rate $\frac{d\alpha}{dt}$ versus α, while the kinetic paramenters A and E_a can be obtained by linear regression of Arrhenius plots based on either derivative or integral data.

The kinetic paramenters are obtained from the slope and the intercept of the Arrhenius plots:

$$\ln\left(\frac{d\alpha)}{dt}\frac{1}{f(\alpha)}\right) = \ln(A) - \frac{Ea}{R\mathrm{T}} \tag{A6}$$

where the values of $\frac{d\alpha}{dt}$ are taken at fixed conversion degree (α) from the different TG experiments at isothermal temperature T.

If integral methods are used, instead, the Arrhemius plots are based on average conversion rate ($R_{av=}\frac{\alpha}{\tau}$.), where τ is the timne needed at a given isothermal reaction temperature to accomplish the coinversion degree α .

The particle size and the reaction temperature must be kept sufficiently low to minimize external and internal temperature and concentration gradients so as to guarantee that reaction occurs under kinetic control. In this case the Arrhenius plots are linear and a linear regression allows to estimates the values of A and E_a

From non-isothermal TGA experimental campaigns

A fast and simple way to obtain approximate values of the kinetic paramenters from a single non-isothermal thermogravimetric (NI-TG) experiment is still through Eq. (8). In this case the values of $\ln\left(\frac{d\alpha}{dt}\frac{1}{f(\alpha)}\right)$ to be plotted are obtained throughout the non-isothermal experiment as a function of the increasing temperature.

İf heat and mass transfer limitations are negligible, the Arrhenius plot shows a linear region from which, through linear regression, it is possible to estimates the value of A and E_a just the way it is done from isothermal thermogravimetric campaigns. This method requires a preliminary decision on the functionality of $f(\alpha)$. This functionality can be in first approximatiom set to $(1-\alpha)$ otherwise could be obtained from the trend of $\frac{d\alpha}{dt}$ versus (α) in an isothermal thermogravimetric test. Thus the minimum set of experiments necessary to derive a simple kinetic rate expression is constituited by a non-isothermal plus an isothermal thermogravimetric experiment carried out under kinetic control.

Several more accurate, yet more complex, methods have been developed to perform kinetic analysis from non-isothermal thermogravimetric campaigns [30,66–73], such as as the methods of Kissinger [66], Friedman [67], Kissinger–Akahira–Sunose (KAS) [68], Flynn–Wall–Ozawa (FWO) [69–70], Coats–Redfern (CR) [72], Starink [73], which methods are often implemented in thermogravimetric analysis software packages and have been routinely applied in many recent papers.

The main features of common non-isothermal kinetic analysis methods are summarized in Table A2. While further details on these models can be found in [66–73] it must be remarked that all of them work fine for reactions characterized by a single component and a well-defined stage of mass loss. In such simple situation, indeed, even the simple Kissinger method, which assumes a single value of activation energy, provides good estimates of the kinetic parameters. The analysis is more complex when multiple reactions occur in parallel and series.

A.3 Kinetics for parallel reactions

Lignocellulosic biomass are composite materials, made of hemicellulose, cellulose, lignin, plus smaller amounts of extractives and other species. Results of thermogravimetric analysis generally reveal the existence of multiple stages of weight loss, which, as remarked before, makes the kinetic analysis from thermogravimetric curves a rather complex job.

Assuming that the sample is composed of i components with weight fraction y_i and that these components undergo parallel-non interacting reactions, Eq. (A1) becomes:

$$\frac{d\alpha}{dt} = \sum_i \frac{d\alpha_i}{dt}y_i = \sum_i A_i e^{-\frac{Eai}{RT}}f(a_i)y_i \tag{A7}$$

If the difference between the rates of the single reactions is large enough, the TG pattern is characterized by well-resolved and distinguishable stages of weight loss. In this case, the kinetic parameters can be well resolved by the iso-coversional methods described before.

Otherwise, the parameters of the kinetic expression Eq. (A5) must be assessed by least squares fitting of experimental TG/DTG curves, even though it is still advisable to perform a preliminary analysis by the iso-conversional methods, in order to get first estimates of the activation energy values [68]. For reaction schemes with a large number of parallel reactions, the DAEM kinetic approach proposed by Vand [89] and further simplified to be applied to biomass pyrolysis, can also be utilized.

References

[1] IPCC Report, https://www.ipcc.ch/sr15/.
[2] Avanade's S, Rodat S, Boujjat H. Solar thermochemical green fuels production: A review of biomass pyro-gasification, solar reactor concepts and modelling methods. Energies 2021:14(5):1494.
[3] Álvarez L, Gil MV, Riaza J, Pevida C, Rubiera F. Fundamentals of oxy-fuel carbon capture technology for pulverized fuel boilers combustion: types of reactions. Fundam Process Adv Technol 2014:169–97.
[4] Anca-Couce A. Reaction mechanisms and multi-scale modelling of lignocellulosic biomass pyrolysis. Prog Energy Combust Sci 2016;53:41–79.
[5] Babu BV. Biomass pyrolysis: a state-of-the-art review. Biofuels Bioprod Bioref 2008;2(5):393–414.
[6] Cai Y, Tay K, Zheng Z, Yang W, Wang H, Zeng G, et al. Modeling of ash formation and deposition processes in coal and biomass fired boilers: a comprehensive review. Appl Energy 2018;230:1447–544.
[7] Choi C, Zhang W, Fukumoto K, Machida H, Norinaga K. A review on detailed kinetic modeling and computational fluid dynamics of thermochemical processes of solid fuels. Energy Fuels 2021;35:5479–94.
[8] Dernbecher A, Dieguez-Alonso A, Ortwein A, Tabet F. Review on modelling approaches based on computational fluid dynamics for biomass combustion systems. J Sci Food Agric 2019;9:129–82.
[9] Di Blasi C. Combustion and gasification rates of lignocellulosic chars. Prog Energy Comb Sci 2009;35(2):121–40.
[10] Di Blasi C. Modeling chemical and physical processes of wood and biomass pyrolysis. Prog Energy Combust Sci 2008;34:47–90.
[11] Fatehi H, Weng W, Li Z, Bai XS, Aldén M. Recent development in numerical simulations and experimental studies of biomass thermochemical conversion. Energy Fuels 2021;35(9):6940–63.
[12] Haberle I, Skreiberg Ø, Łazar J, Haugen NEL. Numerical models for thermochemical degradation of thermally thick woody biomass, and their application in domestic wood heating appliances and grate furnaces. Prog Energy Combust Sci 2017;63:204–52.
[13] Hosseini Rahdar MH, Nasiri F, Lee B. A review of numerical modeling and experimental analysis of combustion in moving grate biomass combustors. Energy Fuels 2019;33:9367–402.
[14] Kleinhans U, Wieland C, Frandsen FJ, Spliethoff H. Ash formation and deposition in coal and biomass fired combustion systems: progress and challenges in the field of ash particle sticking and rebound behavior. Prog Energy Comb Sci 2018;68:65–168.
[15] Leng L, Yang L, Chen J, Leng S, Li H, Li H, et al. A review on pyrolysis of protein-rich biomass: nitrogen transformation. Bioresour Technol 2020;315:123801.
[16] Lewandowski WM, Ryms M, Kosakowski W. Thermal biomass conversion: A review. Processes 2020:8(5): 516.
[17] Mazaheri N, Akbarzadeh AH, Madadian E, Lefsrud M. Systematic review of research guidelines for numerical simulation of biomass gasification for bioenergy production. Energy Convers Managem 2019;183:671–88.
[18] Miao Q, Zhu J, Barghi S, Wu C, Yin X, Zhou Z. Modeling biomass gasification in circulating fluidized beds. Renew Energy 2013;50:655–61.
[19] Niu Y, Tan H, Hui S. Ash-related issues during biomass combustion: Alkali-induced slagging, silicate melt-induced slagging (ash fusion), agglomeration, corrosion, ash utilization, and related countermeasures. Progr Energy Comb Sci 2016;52:1–61.
[20] Pourkashanian M, Ma L, Porter R, Edge P, Black S, Clement A, et al. Challenges and opportunities in simulation of coal and biomass combustion in power plants. Proc Int Symp Turbulence Heat Mass Transfer 2015:45–71.
[21] Rabaçal M, Pereira S, Costa M. Review of pulverized combustion of non-woody residues. Energy Fuels 2018;32:4069–95.
[22] Sharifzadeh M, Sadeqzadeh M, Guo M, Borhani TN, Murthy Konda N, Garcia MC, et al. The multi-scale challenges of biomass fast pyrolysis and bio-oil upgrading: review of the state of art and future research directions. Prog Energy Combust Sci 2019;71:1–80.
[23] Van de Velden M, Baeyens J, Dougan B, McMurdo A. Investigation of operational parameters for an industrial CFB combustor of coal, biomass and sludge. China Particuol 2007;5(4):247–54.
[24] Verma AM, Kishore N. A succinct review on upgrading of lignin-derived bio-oil model components. Green Energy Technol 2018:315–34.
[25] Wang S, Dai G, Yang H, Luo Z. Lignocellulosic biomass pyrolysis mechanism: a state-of-the-art review. Prog Energy Comb Sci 2017;62:33–86.
[26] Wang S, Li Q, Zhang H, Yuan H, Yang H, Wang C, Yu Y, Wang K. Virtual Special Issue of Recent Research Advances in China: Thermochemical Processing of Biomass and Solid Wastes. Energy Fuels 2021:35 (3):1885-1889.
[27] Álvarez A, Pizarro C, García R, Bueno JL, Lavín AG. Determination of kinetic parameters for biomass combustion. Bioresour Technol 2016;216:36–43.
[28] Buratti C, Barbanera M, Bartocci P, Fantozzi F. Thermogravimetric analysis of the behavior of sub-bituminous coal and cellulosic ethanol residue during co-combustion. Bioresour Technol 2015;186:154–62.
[29] Cai H, Zou H, Liu J, Xie W, Kuo J, Buyukada M, et al. Thermal degradations and processes of waste tea and tea leaves via TG-FTIR: Combustion performances, kinetics, thermodynamics, products and optimization. Bioresour Technol 2018;268:715–25.
[30] Deng S, Wang X, Zhang J, Liu Z, Mikulčić H, Vujanović M, et al. A kinetic study on the catalysis of KCl, K2SO4, and K2CO3 during oxy-biomass combustion. J Environ Manage 2018;218:50–8.
[31] Garcia-Maraver A, Perez-Jimenez JA, Serrano-Bernardo F, Zamorano M. Determination and comparison of combustion kinetics parameters of agricultural biomass from olive trees. Renew Energy 2015;83:897–904.
[32] Guizani C, Haddad K, Jeguirim M, Colin B, Limousy L. Combustion characteristics and kinetics of torrefied olive pomace. Energy 2016;107:453–63.
[33] Huang X, Rein G. Thermochemical conversion of biomass in smouldering combustion across scales: the roles of heterogeneous kinetics, oxygen and transport phenomena. Bioresour Technol 2016;207:409–21.
[34] Islam MA, Auta M, Kabir G, Hameed BH. A thermogravimetric analysis of the combustion kinetics of karanja (pongamia pinnata) fruit hulls char. Bioresour Technol 2016;200:335–41.
[35] Jayaraman K, Kok MV, Gokalp I. Thermogravimetric and mass spectrometric (TG-MS) analysis and kinetics of coal-biomass blends. Renew Energy 2017;101:293–300.
[36] Kok MV, Ozgur E. Characterization of lignocellulose biomass and model compounds by thermogravimetry. Energy Sources, Part A 2017;39(2):134–9.
[37] Liang F, Wang R, Jiang C, Yang X, Zhang T, Hu W, et al. Investigating co-combustion characteristics of bamboo and wood. Bioresour Technol 2017;243:556–65.
[38] Lopes FCR, Tannous K, Rueda-Ordóñez YJ. Combustion reaction kinetics of guarana seed residue applying iso-conversional methods and consecutive reaction scheme. Bioresour Technol 2016;219:392–402.
[39] López-González D, Avalos-Ramirez A, Giroir-Fendler A, Godbout S, Fernandez-Lopez M, Sanchez-Silva L, et al. Combustion kinetic study of woody and herbaceous crops by thermal analysis coupled to mass spectrometry. Energy 2015;90:1626–35.
[40] Toptas A, Yildirim Y, Duman G, Yanik J. Combustion behavior of different kinds of torrefied biomass and their blends with lignite. Bioresour Technol 2015;177:328–36.
[41] Wang D, Luo S, Zhou Y, Yi C.(2018). Thermogravimetric study of combustion of biomass and anthracite coal by iso-conversional method. J. Iron Steel Res. Int. 2018:25(3): 330–339.
[42] Wilk M, Magdziarz A, Gajek M, Zajemska M, Jayaraman K, Gokalp I. Combustion and kinetic parameters estimation of torrefied pine, acacia and miscanthus giganteus using experimental and modelling techniques. Bioresour Technol 2017;243:304–14.
[43] Xu X, Pan R, Chen R. Combustion characteristics, kinetics, and thermodynamics of pine wood through thermogravimetric analysis. Appl Biochem Biotechnol 2021;193(5):1427–46.
[44] Yu D, Chen M, Wei Y, Niu S, Xue F. An assessment on co-combustion characteristics of chinese lignite and eucalyptus bark with TG-MS technique. Powder Technol 2016;294:463–71.
[45] Liu X, Chen M, Wei Y. Kinetics based on two-stage scheme for co-combustion of herbaceous biomass and bituminous coal. Fuel 2015;143:577–85.
[46] Zhang L, Duan F, Huang Y. Thermogravimetric investigation on characteristic of biomass combustion under the effect of organic calcium compounds. Bioresour Technol 2015;175:174–81.
[47] Zhang S, Chen T, Li W, Dong Q, Xiong Y. Physicochemical properties and combustion behavior of duckweed during wet torrefaction. Bioresour Technol 2016;218:1157–62.
[48] Zhou C, Liu G, Wang X, Qi C, Hu Y. Combustion characteristics and arsenic retention during co-combustion of agricultural biomass and bituminous coal. Bioresour Technol 2016;214:218–24.
[49] Zhou C, Liu G, Fang T, Sing Lam PK. Investigation on thermal and trace element characteristics during co-combustion biomass with coal gangue. Bioresour Technol 2015;175:454–62.
[50] Barzegar R, Yozgatligil A, Olgun H, Atimtay AT. TGA and kinetic study of different torrefaction conditions of wood biomass under air and oxy-fuel combustion atmospheres. J Energy Instit 2010;93(3):889–98.
[51] Deng S, Lu X, Tan H, Wang X, Xiong X. Effects of a combination of biomass addition and atmosphere on combustion characteristics and kinetics of oily sludge. Biomass Convers Biorefin 2021;11(2):393–407.
[52] Huang L, Liu J, He Y, Sun S, Chen J, Sun J, et al. Thermodynamics and kinetics parameters of co-combustion between sewage sludge and water hyacinth in CO2/O2 atmosphere as biomass to solid biofuel. Bioresour Technol 2016;218:631–42.
[53] Sher F, Iqbal SZ, Liu H, Imran M, Snape CE. Thermal and kinetic analysis of diverse biomass fuels under different reaction environment: a way forward to renewable energy sources. Energy Convers Manage 2020;203:112266.
[54] Wu X, Wei Z, Liu J, Chen Z, Evrendilek F, Huang W. Oxy-fuel and air combustion performances and gas-to-ash products of aboveground and belowground biomass of sedum alfredii hance. Chem Eng J 2021;422:130312.
[55] Kopczyński M, Plis A, Zuwała J. Thermogravimetric and kinetic analysis of raw and torrefied biomass combustion. Chem and Proc Eng 2015;36(2):209–23.
[56] Hu J, Song Y, Liu J, Evrendilek F, Buyukada M, Yan Y, et al. Combustions of torrefaction-pretreated bamboo forest residues: physicochemical properties, evolved gases, and kinetic mechanisms. Bioresour Technol 2020;304:122960.
[57] Magdziarz A, Wilk M, Straka R. Combustion process of torrefied wood biomass: a kinetic study. J Therm Anal Calorim 2017;127(2):1339–49.
[58] Li J, Bonvicini G, Biagini E, Yang W, Tognotti L. Characterization of high-temperature rapid char oxidation of raw and torrefied biomass fuels. Fuel 2015;143:492–8.
[59] Apicella B, Russo C, Ciajolo A, Cortese L, Cerciello F, Stanzione F, et al. High temperature pyrolysis of lignite and synthetic carbons. Fuel 2019;241:264–72.
[60] Senneca O, Apicella B, Russo C, Cerciello F, Salatino P, Heuer S, et al. Pyrolysis and thermal annealing of coal and biomass in CO2-rich atmospheres. Energy Fuels 2018;32(10):10701–8.
[61] Senneca O, Ontyd C, Cerciello F, Schiemann M, Scherer V. Extension of the thermal annealing concepts developed for coal combustion to conversion of lignocellulosic biomass. Energy Fuels 2020;34(3):3661–70.

[62] Senneca O, Cerciello F, Russo C, Wütscher A, Muhler M, Apicella B. Thermal treatment of lignin, cellulose and hemicellulose in nitrogen and carbon dioxide. Fuel 2020;271:117656.
[63] Cerciello F, Apicella B, Russo C, Cortese L, Senneca O. Effects of pressure on lignocellulosic biomass fast pyrolysis in nitrogen and carbon dioxide. Fuel 2021; 287:119604.
[64] Senneca O, Cerciello F, Cortese L, Heuer S, Schiemann M, Scherer V. Effects of CO2 enriched atmosphere on chars from walnut shells pyrolysis in a drop tube reactor. Fuel 2018;229:235–40.
[65] Li Y, Li B, Du F, Xian X, Huang H, Tang P. Structure and combustion characteristics of lignin from black liquor of bagasse soda pulping. CIESC J 2017;68(1):345–52.
[66] Kissinger HE. Variation of peak temperature with heating rate in differential thermal analysis. J Res Natl Bur Stand 1956;54:217–21.
[67] Friedman HL. New methods for evaluating kinetic parameters from thermal analysis data. J Polym Sci Part B Polym 1969;7:41–6.
[68] Akahira T, Sunose T. Joint convention of four electrical institutes. Sci Technol 1971;16:22–31.
[69] Ozawa T. A new method of analyzing thermogravimetric data. Bull Chem Soc Jpn 1965;38:1881–6.
[70] Flynn JH, Wall LA. A quick, direct method for the determinatiovn of activation energy from thermogravimetric data. J Polym Sci Part B Polym 1966;4:323–8.
[71] Doyle CD. Estimating isothermal life from thermogravimetric data. J Appl Polym Sci 1962;6(24):639–42.
[72] Coats AW, Redfern JP. Kinetic parameters from thermogravimetric data. Nature 1964;201:68–9.
[73] Starink MJ. The determination of activation energy from linear heating rate experiments: a comparison of the accuracy of isoconversion methods. Thermochim. Acta 2033:404: 163-176.
[74] Senneca O, Chirore R, Salaytino P. Oxidative pyrolysis of solid fuels. J Anal Appl Pyrolysis 2004;71(2):959–70.
[75] Vyazovkin S, Burnham AK, Criado JM, Pérez-Maqueda LA, Popescu C, Sbirrazzuoli N.ICTAC Kinetics Committee recommendations for performing kinetic computations on thermal analysis data.Thermochim. Acta 2011 (520):1-19.
[76] Vyazovkin S, Chrissafis K, Di Lorenzo ML, Koga N, Pijolat M, Roduit B, et al. ICTAC kinetics committee recommendations for collecting experimental thermal analysis data for kinetic computations. Thermochim Acta 2014;590:1–23.
[77] Vyazovkin S, Burnham AK, Favergeon L, Koga N, Moukhina E, Pérez-Maqueda LA, et al. ICTAC Kinetics Committee recommendations for analysis of multi-step kinetics. Thermochim Acta 2020;689:178597.
[78] Barrie PJ. The mathematical origins of the kinetic compensation effect: 1. the effect of random experimental errors. Phys Chem Chem Phys 2012;14:318–26.
[79] Liu N, Wang B, Fan W. Kinetic compensation effect in the thermal decomposition of biomass in air atmosphere. Fire Saf Sci 2003;7:581–92.
[80] Kreitzberg T, Wirch N, Bormann C, Pielsticker S, Hatzfeld O, Mayer J, et al. Thermally induced changes in microstructure and reactivity of biogenic and fossil fuel particles. Appl Energy 2019;254:113607.
[81] Lester E, Avila C, Pang CH, Williams O, Perkins J, Gaddipatti S, et al. A proposed biomass char classification system. Fuel 2018;232:845–54.
[82] Vorobiev N, Becker A, Kruggel-Emden H, Panahi A, Levendis YA, Schiemann M. Particle shape and Stefan flow effects on the burning rate of torrefied biomass. Fuel 2017;210:107–20.
[83] Liang D, Singer S. Pore-resolving simulations to study the impacts of char morphology on zone II combustion and effectiveness factor models. Combust Flame 2021;229:111405.
[84] Oo HM, Karin P, Chollacoop N, Hanamura K. Physicochemical characterization of forest and sugarcane leaf combustion's particulate matters using electron microscopy, EDS XRD and TGA. J Environ Sci 2021;99:296–310.
[85] Wang P, Zhang J, Shao Q, Wang G. Physicochemical properties evolution of chars from palm kernel shell pyrolysis. J Therm Analy Calorim 2018;133(3):1271–80.
[86] Yu J, Sun L, Berrueco C, Fidalgo B, Paterson N, Millan M. Influence of temperature and particle size on structural characteristics of chars from beechwood pyrolysis. J Anal Appl Pyrolysis 2018;2018(130):249–55.
[87] Ontyd C, Pielsticker S,Yildiz C, Schiemann M, Hatzfeld O, Ströhle J, Epple B, Kneer R. Scherer V. Experimental determination of walnut shell pyrolysis kinetics in N_2 and CO_2 via thermogravimetric analysis, fluidized bed and drop tube reactors. Fuel 2021 (287): 119313.
[88] Deng BL, Yang X, Li M, Cai-Ping W, Bin LW, Chi-Min S. Combustion properties of coal gangue using thermogravimetry–Fourier transform infrared spectroscopy. Appl Therm Eng 2017;116:244–52.
[89] Vand V. A theory of irreversible electrical resistance changes of metallic films evaporated in vacuum. Proc.Phys.Soc. 1943 (55): 222-246.